AFCRL 65-855 (I)

AD632416

AN INVESTIGATION OF PROPERTIES OF THE LASER MICROPROBE

by

JAMES J. DEVLIN, S.J.

and

ANTHONY B. LA CONTI

BOSTON COLLEGE

CHESTNUT HILL, MASSACHUSETTS

CONTRACT NO. AF19(604)-8819

PROJECT 5620

TASK 562003

FINAL REPORT (PART I)

13 August 1965

Period Covered   1 July 1964   to   13 August 196

Prepared for

AIR FORCE CAMBRIDGE RESEARCH LABORATORIES
OFFICE OF AEROSPACE RESEARCH
UNITED STATES AIR FORCE
BEDFORD, MASSACHUSETTS

Requests for additional copies by agencies of the Department

of Defense, their contractors, or other government agencies should be

directed to:

> Defense Documentation Center (DDC)
> Cameron Station
> Alexandria, Virginia 22314

Department of Defense contractors must be established for

DDC services or have their "need-to-know" certified by

the cognizant military agency of their project or contract.

Unclassified reports, OTHER THAN REPRINTS OF JOURNAL

ARTICLES USED AS SCIENTIFIC OR FINAL REPORTS shall display

the following additional information under the above notice:

All other persons and organizations should apply to the:

> Clearinghouse for Federal Scientific
>   and Technical Information (CFSTI)
> Silis Building
> 5285 Port Royal Road
> Springfield, Virginia 22151

ABSTRACT

An investigation of the Laser Microprobe as a source for emission spectrochemical analysis is reported. The size and character of the crater: burnt into a number of pure element metals was investigated. Working curves for a series of iron and aluminum alloys were produced. This gave a measure of the sensitivity and reproducibility of the Laser Microprobe.

INTRODUCTION

The purpose of this research project was the scientific investigation of Laser Microprobe[1] as a source for spectrochemical analysis. This source was manufactured by the Jarrell-Ash Co, of Waltham, Massachusetts. The principal properties of any spectrographic source are it radiant power output, its sensitivity and reproducibility. The latter two properties are especially important for quantitative spectrochemical analysis.

Two types of standard samples were used in this investigation one steel and the other aluminum. These were chose because reliable standards are available for both of these alloys and because the wide use of spectrochemical analysis of these alloys affords a sound reference point for the properties of the Laser Microprobe.

BACKGROUND MATERIAL

Since the Laser is not a device well known to spectroscopists a short discussion of the Theory of Ruby Laser is inserted at this point.

Natural or synthetic ruby is αAl_2O_3 containing some Cr^{+3} ions in place of Al^{+3}. The Cr^{+3} present as the oxide has the symmetry of a slightly distorted octahedron. The absorption spectra of pink ruby containing 0.05%. Cr_2O_3 is given in Figure I. There are two wide, intense bands at approximately 25,000 and 18,000 cm^{-1}, and a sharp, weak doublet at about 13,000 cm^{-1}. The transitions to which these bands correspond are given directly above the peaks. Figure 2 can be used to explain the intensity and width of the bands.

We may regard the coordinate Q as the distance between the chromium and the nearest neighbor ions. A sharp absorption line results from a transition to the $t_{2g}^3(^2E)$ state, and broad absorption bands in the blue and green region correspond to transitions to the $t_{2g}^2 e_g (^4T_2)$, and $t_{2g}^2 e_g (^4T_1)$ states respectively. The designations of the states of the ion in the crystal field are the Mulliken symbols.[2]

Important features in this figure are as follows: The energy curves of the ground state and ^2E states are parallel to each other because of the same electron configuration associated with them, t_{2g}^3. Because of this, a transition to the ^2E state will give rise to an extremely sharp line. The minimum positions of the $^4T_2$ and $^4T_1$ states are displaced from the minimum of the ground state, and the curvature of these curves are not necessarily equal to that of the ground state. This fact can be ascribed to the electron configuration associated with the excited quartet states being different from that of the ground state. The displacement of the energy minima of the excited quartet states is evidenced by the observed broadness of the absorption band widths (Frank-Condon Principle). In such circumstances the energy curve of the excited quartet states cross those of the excited doublet and the ground state, while the energy curve of the doublet state does not cross the ground state energy curve. The sharp doublet arising from a transition to the ^2E state plays a key role in operation of the ruby laser.

There is a quantum mechanical selection rule which states that transitions between states of different spin multiplicaties are highly improbable. When such transitions do take place the intensity of the absorption band or bands usually are very weak. The absorption bands arising from the $^4A_2-^2E$ transition are very sharp and weak.

The first laser built was of a single crystal of pink ruby (0.05% Cr_2O_3), by Maiman in 1960.[3] Stimulated emission was observed at a wave-length of 6943 A°. Many other materials capable of laser action have been built since Maiman's discovery, however, with minor modifications the ruby laser is the most rugged and powerful source of monochromatic light. The oscillator strengths of the absorption bands in ruby are of the order of magnitude of 10^{-4} to 10^{-3} and their broadness is convenient for optical pumping. The presence of an intermediate metastable state with a lifetime of 3 to 4 milliseconds makes ruby an ideal laser material.

To obtain laser action, a cylindrical sample of ruby whose ends are polished optically flat, parallel, and partially silvered is irradiated with light from a helical xenon flashlamp. Figure 3 can be used to explain how laser action takes place in ruby. Electrons in the $^4A_2$ ground state are raised to the $^4T_1$ and $^4T_2$ excited states. A rapid non-radiative decay of electrons in the excited quartet states to the ^2E metastable state occurs by loss of energy to the crystal lattice in the form of vibrations. The purpose of the flashlamp is to obtain more electrons in the metastable ^2E state than in the ground state. When the critical population inversion is reached, an atom while it is still excited can be stimulated to emit a photon if it is struck by an outside photon having precisely the energy of the one that would be emitted spontaneously. As a result the incoming photon is augmented by the one given up by the excited atom. The wave upon release falls precisely in phase with the wave that triggered its release.

The waves are reflected back and forth through the cavity stimulating other excited chromium atoms to emit light in the same direction and phase. Within a few billionths of a second this chain reaction builds up such a powerful beam that it bursts our of the partially silvered end. Stimulated emission occurs at a wavelength of 6943A°. The beam of light is highly monochromatic, directional, and coherent. There must be an excess of excited atoms to enable stimulated emission to predominate over absorption.

The coherence of light generated by the laser is its most useful property. Coherent light waves possess traveling surfaces of constant phase moving in an extremely narrow beam. The amplitude and phase of coherent light can be specified closely.

Ordinary lasers such as those constructed by Maiman (2) emit peak powers of the order of milliwatts in pulses lasting about a millisecond. The pulse shape and power is irregular. Figure 4 shows the flashlamp and laser radiation for a non Q-spoiled ruby laser The events in the diagram are simultaneous and have the same unit of time, namely milliseconds. The ordinate represents the intensity of radiation in relative units. The intensity of the flashlamp radiation is much weaker than that of the laser.

Hellworth and McClung (4) found a way to remove these irregularities parially and at the same time increase the peak intensity. Their method of controlling the regeneration process is called Q-spoiling. It consists of employing an optical shutter within the laser cavity to obtain a giant pulse with peak power in the order of megawatts lasting approximately 50 nanoseconds (50×10^{-9} seconds).

g

Instrumentation

.

The Laser Microprobe uses the mechanical rotation of one
of the terminal mirrors as a basic shutter mechanism. It has the
following characteristics: The cross sectional area of the ruby
face is decreased from earlier rods to aid in focusing to a smaller
spot. To keep the number of chromium atoms available for excita-
tion virtually the same, the chromium content of ruby has been
increased from 0.05 to 0.5%. The rod is 75 mm long and 6 mm in
diameter. It has a Brewster angle window aligned with a 90°
prism reflector rotating at 18,000 r.p.m. (optule), and a double
sapphire window that provides 55% reflectance at 6943Å. The
laser rod is pumped by a helical xenon flashlamp rated at 4 KV

r.

and a variable output up to 1000 joules is delivered in 1.0
milliseconds, from a 150 μf (microfaraday) power supply rated
for use at a 4 KV. A multitapped inductance is used as a com-
ponent of the pulse shaping network. The electrical energy is
pumped into the optical flashtube by a triggering pulse synchron-

--

ized to the optule. The peak power of a single pulse is about

r

3 megawatts and the duration is as long as 100 nanoseconds.
Divergence of radiation is less than 2 milliradians. The laser
beam is focused onto a sample by using a prism to reflect the
laser beam through a Cooke metallurgical five lens microscope
with a focal length of 12.5 mm and resolving power of 2.5 microns.
Figure 5 illustrates the main features of the instrument.

A 3/4 meter high aperture spectrograph with a speed of F/6.3 containing a 57,000 lines per inch grating and Czerney-Turner mount is used along with Eastman Kodak 103-0 plates to record the spectra. The Czerney-Turner mounting for monochromators is illustrated in Figure 5. The combination of an extremely fast spectrograph and the 103-0 plates is necessary to record the spectra produced when the focused laser light interacts with a solid. The line intensity was measured with a Jarrell Ash 23-100 recording microphotometer.

It is advantageous to monitor the output of the laser without significantly affecting the interaction process. In order to do this a glass microscope plate was placed at a 45° angle between the prism and the laser source. Four percent of the laser light was reflected 90° upward. By fusing a second glass plate at a 90° angle to the first, it becomes possible to reflect 0.16% of the laser light to a photodetector with a very fast response time which is placed directly above the laser source. So as not to overload the photodetector with light it is necessary to attenuate the laser beam with a filter having a density of 3.6. A blackened photographic film was used as a filter. The observed pulse shape was displayed onto a Tektronix 535A oscilloscope containing a type A plug-in unit. The arrangement of the laser monitoring system, and the electronic schematic of the photodetector are also given in Figure 5.

With the Laser Microprobe it is possible to obtain a single pulse of light with a 45 nanosecond duration. About 96% of this

light is used to evaporate and excite a solid sample. The remaining 4% of the light is reflected, and attenuated so that 0.5 watts of laser light strike the surface of a suitably biased EGG SD-100 photodiode. This causes 0.12 amperes of current to flow through the circuit. The IR drop developed across the 50 ohm resistor is about 6 volts. This signal is displayed onto a Tektronix 535A oscilliscope having a 10 nanosecond rise time. From the voltage signal displayed on the oscilliscope, the peak power of a single pulse was calculated as being approximately 2 megawatts. The RC time constant of the laser detector is about 3 nanoseconds ($R=200$ ohms, $C=1.6 \times 10^{-12}$ faradays).

Some of the practical problems encountered with the Laser Microprobe are pitting of the multilayer dielectric reflectors; occasional splashing of the solid sample onto the lower microscope lens; and fogging and eventual pitting of the upper two lenses of the microscope. The multilayer reflectors are now made of sapphire to cope with the high peak powers. The lower microscope lens can be covered with a piece of "Mylar" which can be replaced weekly. To avoid the fogging and eventual pitting of the upper two lenses, the cement is removed from between the lenses with toluene.

Experimental Observations of the Interaction

of Laser Light with Solids

Early in 1962 the Jarrell Ash Company and Lear Siegler Company
(formerly Trion) developed the Laser Microprobe. By performing some
applied research with this instrument, Jarrell Ash developed it into a
qualitative tool for emission spectroscopy. With this tool, the emission of
light by the sample is stimulated by focusing the coherent radiation from a
ruby laser through a microscope to a place where the solid sample is located.
This very high concentration of light generates intense local heat, and vaporizes
a sample in a fraction of a second. Cross excitation of the sample vapor is
provided by the self-triggering of a gap between two electrodes kept under high
voltage which causes further excitation of the already partially excited vapor.
By superimposing several cross excited laser shots, an emission spectrum can
be obtained with any commercially available spectrograph. Most of the research
on the use of the laser in emission spectroscopy was performed with the Laser
Microprobe using the auxiliary cross excitation [1]. The prime concern of
the researchers was application.

The major objection with performing any basic research with the system
just described is that the laser and spark excitation are combined. The spectra
produced by this method is not very reproducible because of the many variables
entering into the two combined excitation processes. Difficulties are caused
by the introduction of impurities present in carbon electrodes into the vapor.
Also several regions of the spectrum are made unavailable because interfering
emission lines and bands are emitted by the electrodes during excitation. The
Laser Microprobe is used without cross electrodes for this research program
so the only excitation of vapor is that produced by the laser.

The primary concern of the research is not on the application of laser induced spectral analysis. A study is made on the mechanisms and factors entering into the interaction and excitation processes which affect quantitative analysis by the laser. A quantitative analysis of aluminum and iron alloys with the simple laser is performed.

In the experimental work the first effort was directed toward a study of the impact of the light pulse on various materials. The pulse shape and power of the Laser Microprobe is monitored with the equipment shown in Figure 5. The pulse shape and power of the Laser Microprobe depends on the power applied to the 150 uf power supply. An increase in joules input leads to an increase in joules output (Table I). Figures 6A and 6B illustrate the change in the pulse shape as the voltage applied to the capacitor bank is increased. The threshold voltage is 3050 volts. Up to 200 volts beyond threshold a reproducible single pulse is produced. At 3300 volts the pulse shape changes randomly from a single to a multiple spike. There is a variation in pulse shape and total pulse power. At a fixed voltage above 3350 the total power output remains virtually the same, but the pulse shape varies with each firing of the laser. The peak power of a single pulse is about 3 megawatts. The pulse duration and power increase with increasing applied voltage.

When the laser beam is focused on certain pure metals (99.9% or greater purity) all cut to the same dimensions, a small amount of material is melted and vaporized. A multiple spike laser having a total output of approximately 0.7 joule interacted with 19 metals, and produced the crater volumes given in Table II. The reproducibility of the measurements are expressed in terms of coefficient of variation. The crater dimensions given in Table II and the photographs of the laser craters shown in Figures 7A and 7B are obtained with a Carl Zeiss

Ultraphot II microscope with camera attachment. Figure 7A contains
a photograph of the crater diameter measuring scale. The crater
volumes depend on the thermal conductivities and melting points of
the solids. High thermal conductivity and low melting point favor
a large crater volume. The physical properties of the target metals
are given in Table III. The photographs given in Figure 7 indicate
that materials with large craters such as Pb or Al show some spillage
of material, while metals such as Cd, Cu, or Zn show considerable
spillage. For higher melting materials such as Fe and Ta, the photo-
graphs suggest that an explosion took place from within and the
melted material deposited itself on the sides of the crater. These and
other photographs indicate that a large portion of the material that
leaves the craters is in the liquid and solid form.

The energy in joules necessary to vaporize the material within
each crater volume is given in Table IV. The values for the sublim-
ation energies are taken from Honig (5), and are based on vapor pres-
sure measurements. In all cases the available energy (0.7 joule) is
far greater than any of the values found in Table IV.

The data in Table V shows that as the total power output of the
laser increases, there is an increase in the crater diameter for a
given element.

Photographs of the emission lines produced in the region 2500
to 3300A° by direct laser excitation, and cross excitation of the laser
induced vapor by carbon electrodes are given in Figures 8A, 8B, and
8C for all of the elements for which crater volumes are measured. At
0.7 joule output, it was found experimentally that six superimposed
laser shots were needed to bring out the emission lines produced by
direct laser excitation while only one shot was required when the cross
excitation method was used. The emmission lines produced by direct
laser excitation of twelve elements are marked and identified. The
energies required to produce the electron transitions are also recorded
(6). This data is summarized in Table VI.

In Table VI the laser-produced emission lines of twelve elements are compared to those obtained by Corliss and Bozman (7) for the same twelve elements. Corliss and Bozman and Bozman used a Cu arc maintained at 5100° ± 110°K as an excitation medium. Emission lines which appear for both laser and DC Cu arc excitation are marked by a P. If a laser-produced line is self reversed, it is indicated in the first column of the tables by an R.

The emission lines resulting from the arcing of each of the twelve elements in a Cu matrix have very low excitation energies, and seldom exceed 8.0 electron volts (ev). Laser-produced emission lines having excitation energies between 10 and 15 ev are quite common for metals having high melting points or high thermal con-ductivities. Emission lines having excitation energies as high as 20 ev also appear for these metals. Low melting or low thermal conductivities metals exhibit similar emission lines during laser and DC arc excitation. The excitation energies seldom exceed 8 ev. Howe (8), studying the interaction of laser light with carbon, reports temperatures as high as 10,000°K. Honig (9,10) reports surface temperatures of 5600°, 7200, and 9500°K for Ge, Fe and Ta respectively. The vapor temperature reached by high conductivity or high melting metals probably is in excess of 7000°K while that of low melting and low conductivity metals is closer to the Cu arc temperature.

For many of the laser-produced emission lines, the intensity near the center of the line showed self-absorption. Self-absorption was exhibited by all of the metals having large laser-produced crater volumes. For the coinage metals such as Ag, Au and Cu, the self-absorption was less. Elements such as Pt, Fe, or W showed only a limited amount of self-absorption. The widths of the laser-produced spectral lines also decreased in a similar manner.

The emission lines produced by laser interaction are considerably wider than can be explained by Doppler broadening and are probably due to collisional and pressure broadening. For extreme cases of self absorption such as that observed in Figures 8A and 8B, the intensity near the center of the line is almost wholly absorbed. The self absorption is not symmetrical and usually is greatest on the long wavelength side of the line during laser excitation.

Model for Interaction of a Laser Beam with a Solid

For ordinary lasers, the vaporizing process can be described by a conventional boiling treatment (11). When a giant pulse laser beam interacts with a solid, heat absorption occurs too rapidly for a treatment based on conventional boiling to be applicable. For example, if we take the data given in Table IV, and assume that the laser output is 0.7 joules, the crater volumes expected for each of the metals can be calculated from a conventional boiling treatment. No correlation exists between the expected crater volumes and those obtained experimentally.

The vaporization of a solid by a giant pulse laser beam is described adequately, by a phenomenonalogical model given by Ready (11).

Ready tried to estimate the probable temperature of the target surface as a function of time when a Q switched laser of 30 magawatt peak power and 45 nanosecond duration is focused on a carbon block in air. The temperature pulse at the surface of carbon was calculated by solving the equation for linear heat flow when heat is produced in a thin layer near the surface of the material at the rate $\alpha f(t)$ exp. (αx) by laser radiation, where $f(t)$ is the power density of the focused laser beam at the surface of carbon, α is the absorption coefficient of carbon, and x is the distance from the surface (11). The shape of the calculated temperature pulse, and the shape assumed for the laser pulse are given in the above reference.

Ready supports his work on the calculated temperature-time pulse by his high speed camera studies of the development of the laser-produced plume which show a considerable delay between peak surface temperatures and emission of the vaporized material (12). An Electro-Optical Instrument Model KFC-600/B high speed framing camera was used to photograph successive states in the development of the plume produced by the laser interacting with carbon. Photographs taken show the following sequence of events:

Time (nanoseconds)	Photographic Observations
20	No emission
45	Bright spot just appearing
70	Considerable development of the plume
820	Plume diminished in brightness, but still appearing.

Similar studies show that the maximum brightness of the plume occurs 120 nanoseconds after the start of the laser pulse, and the plume fades slowly after that. Ready (11) estimates that the velocity of the front surface of the developing plume is 2×10^6 cm/sec..

Ready's (12) photographs show that the emission of vaporized material does not begin until the temperature pulse has declined from its peak value. He interprets this delay as providing tentative support for his phenomenological model of the vaporization produced by a giant pulse laser beam. The essential features of his model are as follows: subsurface particles in the solid reach vaporization temperature before the surface particles have absorbed their latent heat of vaporization. A pulse of high pressure develops and the material is superheated until the temperature reaches above the critical point. At this point there is no longer any distinction between the superheated solid and highly condensed gas. The emission of the vaporized material, which is delayed relative to the peak of the temperature pulse at the surface proceeds like a thermal explosion (12).

When light is absorbed in metals by internal photo effect, electrons are raised to higher energy levels in the conduction band (11).

Heat is produced by collisions of the excited electrons with the lattice. Since the collision times of good conductors are in the order of 10^{-11} to 10^{-13} seconds and the laser pulse durations are in the order of 10^{-9} seconds, the light can be considered as being converted directly to heat. The photographs of the laser-produced craters given in Figure 7 support Ready's vaporization theory (11) that an explosion type phenomenon occurrs from within when the laser light strikes a solid. The vaporization mechanism explains the volumes of the craters reported in Table IV. The depth of penetration of the laser-produced craters probably depends on the melting point and absorption coefficient of the target material for laser light. The crater size will depend on how much energy is used in the melting process, and the amount of time before a thermal explosion takes place. For low melting, high boiling elements such as Pb, In, Sn, and Al the depth of penetration is considerable. For low melting, low boiling elements such as Cd or Zn the depth of penetration is less. The thermal conductivity of the material is very important for it probably prolongs the time before a thermal explosion takes place by transferring heat from hot to cold areas.

The experimental data obtained with the Laser Microprobe elucidates the excitation mechanism in the rising vapor plume. After the thermal explosion, the expanding vapor is optically dense and only surface black body radiation is observed. As the vapor expands outward, the plume becomes optically transparent and line spectra can be seen. Excitation in the rising vapor takes place by joule heating and the inelastic collisions of atoms and electrons in vaporized material of high temperature and low volume. Because of the high pressure and the constricted volume, there is a large amount of collisional and pressure broadening of the emission lines. Surrounding the central hot core of the expanding vapor is a cooler outer fringe which contains atoms in the ground or low energy states. Lines of given element radiate out through the absorbing fringe where elements

of the same kind may absorb this radiation, thus many lines are self reversed.

When a multiple pulse laser beam is used for analysis, interaction of the laser light with the rising vapor plume must be considered. The vapor produced by the first spike is still present and radiating 0.5 microseconds after the start of the pulse. Part of the energy of a second spike is consumed in the excitation of the partially radiating vapor produced by the first spikes. The net result is that the integrated intensity of the spectran is greater than would be observed without interaction (Table VII).

Quantitative Analysis of Aluminum Alloys

A quantitative analysis of five different sets of aluminum alloys was performed with a laser and an AC spark source.

Two basic requirements for quantitative spectrochemical analysis, which employs a photographic plate or film as a spectrum recording device, are a calibration curve for the plate or film emulsion, and a working curve for the element whose concentration is sought. A calibration curve for a 103-0 photographic emulsion is given in Figure 10. It was obtained from a sectored iron arc spectrum. The ratio of successive steps of the sector is 1.595 to 1. The conditions and data used for the construction of the calibration curve are given in Table VIII.

Working curves are constructed by plotting the relative intensity ratio of an element spectrum line and a matrix line of equivalent characteristics versus element concentration on a log-log basis. For a particular element the working curve usually changes slope according to the matrix in which the element is found when an AC spark or DC arc is used as an excitation source.

In a paper delivered in College Park Maryland in June 1962, Arno Arrak[13] demonstrated that one of the major causes of changing slopes is the variable surface oxidation rates of alloys which are caused by the presence of different ratio of impurities within the alloy. He eliminated the high temperature surface

oxidation by using an inert atmosphere spark chamber. A so called "black burn" which is indicative of no oxide formation is reported with both nitrogen and argon. Universal analytical curves valid for all ferrous alloys are constructed by sparking low and high alloy steels in nitrogen and argon under conditions producing a black burn. Allowance is made for variations of the internal standard line intensity with iron concentration for the higher alloy steels.

When a laser beam interacts with a solid, the vapor rises so rapidly that the surface oxidation which occurs with a DC arc or an AC spark source does not begin until the material leaves the crater. Curves of impurity concentration against relative intensity should have the same slope as long as the concentration of base material remains virtually the same. Working curves for five impurities present in five different sets of aluminim alloys (%Al > 90) are constructed by using the Al(3059) and Al (3050) as internal standard lines for the spark source and laser source respectively. In Figure 11A to 11E the working curves from the two different sources are compared. Six superimposed laser shots are needed to bring out the laser induced spectra. Table IX gives the concentration of the aluminum alloys. The conditions and data used for the construction of the working curve are tabulated in Table X and XI for the spark source and laser source respectively.

The slopes of the working curves produced by AC spark excitation depend on which set of aluminum standards the impurity element is found. The matrix dependence of the laser-produced

working curves is far less. The experimental results seem to support Arrak's theory that surface oxidation is one of the major causes of changing slopes. Working curves for Cu, Mn, Si, Mg, and Fe are compared. The slopes of the working curves produced by laser excitation are much inferior to the AC spark slopes in all cases. The limit of detection is reduced by a factor of at least ten when the laser is used as a source. In Table XII a comparison is made of the precision obtainable by the two methods. The coefficient of variation is much higher when the laser is used as an excitation source.

The laser induced emission spectra of aluminum alloys contain very few matrix lines suitable for internal standards since many are extremely broadened or self reversed. The iron spectrum shows very little broadening or self reversal, and the matrix lines are plentiful. The "matrix effect" is studied further by constructing working curves for low and medium alloy steels.

Single and Multiple Pulse Operation
for Quantitative Analysis of Iron Alloys

Single and multiple pulse laser beams were used to excite iron alloys. Working curves were prepared for impurity elements present in five different sets of iron alloys.

In Figures 12A to 12D some of the working curves of impurities present in 5 different iron matrices (%Fe > 70) are compared for a 0.12 and 0.65 joule laser. The concentrations of the iron alloys are tabulated in Table XIII. The conditions and data used for the

construction of the working curves are reported in Table XIV and XV for the 0.12 and 0.65 joule laser respectively. The following are the impurity and matrix lines which gave suitable working curves for both single and multiple spikes: Mn(4041.4)/Fe(4014.5): Mo(3864.0)/Fe(3867.2): Ni(3461.7)/Fe(3471.3): Cr(3368.2)/Fe(3370.8). Figure 9 shows the spectra resulting from 3 superimposed laser shots at 0.65 joules.

The slopes produced by the 0.65 joule laser are slightly steeper than the 0.12 joule slopes. This may be due to an increase in line to background ratio caused by the interaction of laser light with the rising vapor plume. The precision obtainable with the two methods is given in Table XVI. A greater precision can be achieved when one superimposes 20 single spike laser shots. This is probably due to a reproducible single laser pulse and a better statistical averaging of the spectra.

The "matrix effect" seems to be absent from both the single and multiple spike operation. However, if a working curve is constructed for the single spike operation it cannot be used when a multiple spike is selected for analysis. If the pulse power is kept constant, the relative intensity ratio does not change when the number of laser shots is varied once the inertia of the emulsion has been overcome. This can be seen if reference is made to Table XVII. If a log-log plot of relative intensity against number of laser shots is made for any one of the four impurity lines studied and its corresponding internal standard line, two parrallel lines are obtained (Figure 13).

It takes 8 superimposed laser spectra to overcome the inertia of the 103-0 emulsion if the total output of the laser is 0.12 joules, and 2 superimposed spectra if the total output of the laser is 0.65 joules.

DISCUSSION

In this project the ruby laser has been utilized as a useful excitation source for quantitative emission spectroscopy. The experimental observations and the possibilities of improving the laser excitation source are discussed.

Conclusions

A quantitative analysis of aluminum and iron alloys was achieved with the Laser Microprobe as an excitation source. The slopes of the working curves for impurity elements present in aluminum and iron alloys are not matrix dependent. Further research could be conducted to improve the precision, sensitivity and detection limits of the laser excitation source.

Quantitative analysis performed by direct laser excitation should be restricted to high melting metals. When the laser beam interacts with high melting metals it produces small craters, and the excited atoms emit a normal spectra. Large craters are produced when the laser beam interacts with low melting or high conductivity metals. In this case excited atoms emit spectral lines which are extremely broadened and self reversed. A model for the interaction and excitation process has been proposed which explains the experimentally observed data. The model holds for both single and multiple pulse operations.

The emission lines produced by laser excitation are very weak and several spectra must be superimposed to overcome the inertia of the emulsion. A fast spectrograph and photographic emulsion must be used to record the resulting spectra. It is very important in quantitative analysis that the pulse shape and power be known, thus the laser output should be monitored.

The pulse shape and power of the Laser Microprobe determines the crater size and intensity of the spectra for a given element. The beam parameters of the Laser Microprobe depend upon the power applied to the power supply capacitors. When the electrical input is less than 250 volts above the threshold voltage a single spike with some trailing light is obtained. If the electrical input is greater than 250 volts above threshold a multiple spike laser beam results, whose pulse shape veries in a random manner.

The shape and power of a single spike laser beam (0.12 joules) can be reproducible (±10%), however, the spectra is so weak that 20 shots must be superimposed to determine impurities present even in fairly high concentrations. The total power output from a multiple spike laser beam (0.65 joules) is fairly reproducible, but the pulse shape changes in a random manner. Three superimposed laser shots at the 0.65 joule level are equivalent to 20 superimposed shots at the 0.12 joule level. Multiple spike operation involves interaction of laser spikes and laser produced vapor so the excitation mechanism will be affected by the pulse shape.

The Laser Microprobe has been utilized as a useful excitation source for quantitative emission spectroscopy. The inherent

excitation mechanism of the ruby laser which is matrix independent provides a strong incentive to continue a research effort to improve the quality of the spectra which it produces. Other analysis which the laser could perform that would be difficult for conventional sources are the analysis of micro inclusions in solids; the analysis of nonconducting solids such as glass, diamond and ceramics; and construction of profile distribution curves for impurities in solids.

Improvements of the Laser-Produced Working Curves and Spectra

The matrix lines of low melting or high conductivity metals show substantial broadening. When measuring the photographic blackening of an emission line the peak transmission values are recorded and converted to intensity readings from a previously prepared emulsion calibration curve. For laser induced excitation a given impurity line may become broader, rather than darker as the concentration of the impurity increases. For these particular lines the integrated area within the transmission curve is more representative of the concentration than the peak transmission. By using an integrater when preparing calibration and working curves it may be possible to improve the slopes of the working curves resulting from laser excitation.

The ability of a gas to retard the expansion of an atomic metal vapor depends on the molecular weight of the gas and metal atoms, and their collisional cross sections. The stopping power of argon is about five times as great as that of nitrogen[14] so

that ground state emission lines which show self reversal in air
may have a normal shape in an argon atmosphere because the vapor
is not allowed to expand and cool. The number of collisions
between atoms is greater in argon since the vapor is confined to
a smaller area; thus, photographic line intensity should increase.
By constructing a high pressure gas chamber and employing a high
molecular weight inert gas such as xenon, it may be possible
to reduce some of the self absorption and line broadening that
occur when a laser interacts with a low melting or high conductivity
metal.

Table I

Changes in Pulse Duration and Power with Increasing

Voltage Input

Applied Voltage	Pulse Duration (Nanoseconds)	Joules 1 Input	Joules Output
3050	no pulse	700	0
3100	40	720	0.03
3150	40	745	0.06
3200	45	770	0.09
3250	50	790	0.12
3350	1000	840	0.30
3480	1500	915	0.54
3600	2000	970	0.64

1. Joules Input $= 1/2 \ CV^2$, where C = 150 uf

Table II

Volume of Craters Produced by a 0.7 Joule Laser Beam

Element	Average[1] Width (Microns)	Coefficient[2] of Variation	Average[1] Depth (Microns)	Coefficient[2] of Variation	Average[3] Volume (10^8) (Cm^3)
In	202	14.2	118	16.1	126.0
Pb	161	6.96	75	16.9	50.8
Sn	129	5.38	54	15.6	23.5
Al	119	7.09	61	20.3	22.6
Mg	119	10.7	60	9.55	22.2
Cd	114	9.30	42	20.8	14.3
Ag	108	8.94	39	24.7	11.9
Cu	100	13.5	39	22.4	10.2
Au	98	12.0	36	10.1	9.05
Zn	98	9.22	35	13.4	8.80
Ge	89	11.9	45	30.0	8.29
Si	89	12.2	36	12.6	7.46
Pd	90	13.4	35	18.3	7.44
Pt	82	15.7	31	18.3	5.45
Ni	81	17.5	30	26.3	5.15
Fe	80	17.0	30	28.1	5.03
Mo	76	15.1	29	23.9	4.37
Ta	74	13.0	28	21.5	4.02
W	75	13.1	28	21.5	4.13

1 Each value represents the mean for 12 laser craters.

2 Coefficient of variation is the standard deviation expressed as a percentage of arithmetic mean (15).

3 Average volume is calculated by assuming a conical shape for the laser crater,

$$V = \pi r^2 h/3$$

where r is the radius, and h is the height of the crater.

Table III

Physical Properties of Certain Elements

Metal	Melting Point(°C)(16)	Boiling Point(°C)(16)	Thermal[1] Conductivity(16)	Ionization Potential(ev)(17)	Atomic[2] Volume (Cm³)(16)
In	156	2000		5.8	15.74
Pb	327	1620	0.08	7.41	18.27
Sn	232	2260	0.16	7.32	16.23
Al	660	2057	1.01(600°C)	5.95	10.00
Mg	651	1107	0.40	7.64	14.00
Cd	312	'768	0.22	8.99	13.0
Ag	961	1950	1.00	7.87	10.3
Cu	1083	2336	0.86(100°-837°C)	7.72	7.1
Au	1063	2600	0.70	9.22	10.2
Zn	419	907	0.27	9.39	9.2
Ge	959	2700		8.13	13.55
Si	1420	2600		8.15	11.4
Pd	1555	2200	0.17	8.3	9.0
Pt	1774	4300	0.17	9.0	9.1
Ni	1455	2900	0.14	7.63	6.7
Fe	1535	3000	0.16	7.90	7.5
Mo	2620	5560	0.35	7.18	9.4
Ta	3027	4100	0.13	7.0	10.9
W	3370	5900	0.35	7.98	9.5

1 Time rate of transfer of heat by conduction, through unit thickness, across unit area for unit difference of temperature. Values in table are given as cal./(sec.)(cm²)(°C/cm).

2 Atomic Volume = (atomic weight of element)/(density).

Table IV

Thermal Data for Certain Elements

Metal	Sublimation Energy(5) (Kcal/mole)	Crater Volume (10^8) (Cm^3)	Energy in Joules[1] Necessary to Evaporate Material in Crater Volume
In	57	126	0.019
Pb	46.8	50.8	0.0055
Sn	72.0	23.5	0.0044
Al	77.5	22.6	0.0074
Mg	35.4	22.2	0.0024
Cd	26.78	14.3	0.0012
Ag	68.2	11.9	0.0033
Cu	81.0	10.2	0.0049
Au	84.7	9.05	0.0032
Zn	31.22	8.80	0.0013
Ge	92	8.29	0.0024
Si	105	7.46	0.0029
Pd	94	7.44	0.0033
Pt	134.8	5.45	0.0034
Ni	101.2	5.15	0.0033
Fe	99	5.03	0.0028
Mo	157.5	4.37	0.0031
Ta	186.8	4.02	0.0029
W	200	4.13	0.0036

1 The values in the last column are calculated from the formula,

$$W = 4.2 \times 10^3 \, \Delta H_s V/v$$

where ΔH_s is the sublimation energy in Kcal/mole, V is the crater volume, and v is the atomic volume (See table VI for atomic volume values).

Table V

Crater Diameter (Microns) as a Function of Joules Output

Joules Output	Pb	Sn	Al	Cd	Cu	Fe
0.12	91	75	74	68	65	35
0.30	121	87	83	81	78	48
0.54	143	118	110	102	91	65
0.65	160	130	120	115	100	80

Table VI

Wavelength Tables of Spectrum Lines Observed

When a 0.7 Joule Multiple Spike Laser Interacts With a Solid

Table VI A -In

Self Reversed Lines	Plate Identification Number (Fig. 8A)	Wavelength (Å)	Excitation Energy(6) (ev)	Lines Present in Cu Arc Spectrum(7)
R	1	2560.2	4.81	P
R	2	2601.8	5.01	P
R	3	2710.3	4.81	P
R	4	2713.9	4.81	P
R	5	2753.9	5.01	P(2775.4)
	6	2836.9		P(2858.1)
	7	2890.2		
R	8	2932.6	4.47	P
	9	2941.1		
	10	2957.0		P
	11	2982.9		
	12	3008.3		
R	13	3039.4	4.1	P
	14	3048.4		
	15	3059.9		
	16	3182.0		
R	17	3256.0	4.1	P
R	18	3258.0	4.1	P

Table VI B - Pb

Self Reversed Lines	Plate Identification Number	Wavelength (Å)	Excitation Energy (ev)	Lines Present in Cu Arc Spectrum
R	1	2577.3	6.09	P
R	2	2613.7 - 2614.2	5.68	P
	3	2628.3 II		P
	4	2657.1	5.60	P
R	5	2663.2		P
R	6	2802.0	5.67	P
R	7	2823.2	5.67	P
R	8	2833.1	4.4	P
R	9	2873.3	5.60	P
	10	3034.0		
R	11	3043.9		
	12	3137.8		
R	13	3176.5		P
	14	3262.4	6.38	

Table VI C - Sn

Self Reversed Lines	Plate Identification Number	Wavelength (Å)	Excitation Energy (ev)	Lines Present in Cu Arc Spectrum
	1	2571.6	5.88	P
	2	2594.4		P
	3	2632.0		
	4	2637.0	6.82	
	5	2660.0		
	6	2661.3	4.86	P
R	7	2706.5	4.78	P
	8	2779.8	5.52	P
	9	2785.0	5.51	P
R	10	2813.6	5.47	P
R	11	2840.0	4.78	P
R	12	2850.6	5.41	P
R	13	2863.3	4.32	P
	14			
	15	2913.5	6.38	P
R	16	3009.2	4.33	P
R	17	3034.1	4.30	P(3032.8)
	18	3141.8	6.06	P
R	19	3175.0	4.33	P
	20	3247.5 Cu		
R	21	3262.3	4.87	P
	22	3274.0 Cu		
	23	3283.5 II	11.06	
	24	3330.6	4.79	P
	25	3352.4		

Table VI D - Al

Self Reversed Lines	Plate Identification Number	Wavelength (Å)	Excitation Energy (ev)	Lines Present in Cu Arc Spectrum
R	1	2568.0	4.81	P
R	2	2575.2	4.81	P
	3	2631.8 II	15.30	
R	4	2652.5	4.66	P
R	5	2660.4	4.66	P
	6	2795.5		
	7	2802.7		
	8	2816.2 II	11.82	
	9	2852.1		
	10	3050.1	7.65	
	11	3054.7	7.65	
	12	3057.2	7.66	
	13	3059.0	7.65	
	14	3060.0	7.65	
	15	3064.3	7.65	
	16	3066.2	7.65	
R	17	3082.2	4.02	P
R	18	3092.7	4.02	P

ᵘ Table VI E - Mg

Self Reversed Lines	Plate Identification Number	Wavelength (Å)	Excitation Energy (ev)	Lines Present in Cu Arc Spectrum
R	1	2776.7	7.17	P
R	2	2778.3		P
R	3	2779.8		P
R	4	2781.4	7.17	P
R	5	2783.0		P
R	6	2790.8 II	8.86	
R	7	2795.5 II	4.43	
R	8	2798.1 II	8.86	
R	9	2802.7 II	4.42	
R	10	2852.1	4.34	P
	11	2915.5		
	12	2928.8 II	8.62	
	13	2936.5 II	8.65	
R	14	3096.9	6.72	
	15	3321.0		P
	16	3336.7	6.43	P

Table VI F - Cd

Self Reversed Lines	Plate Identification Number	Wavelength (Å)	Excitation Energy (ev)	Lines Present in Cu Arc Spectrum
	1	2573.1 II		
	2	2748.6 II	10.28	
	3	2836.9	8.1	P
	4	2881.0	8.1	P
	5	2980.6	8.1	P
	6	3133.2	7.76	P
	7	3250.2 II		
	8	3261.1	3.30	P

Table VI G - Ag

Self Reversed Lines	Plate Identification Number	Wavelength (Å)	Excitation Energy (ev)	Lines Present in Cu Arc Spectrum
	1	2580.7 II	14.98	
	2	2606.2 II	14.94	
	3	2614.6 II	15.51	
	4	2660.5 II	10.36	
	5	2681.4 II	14.98	
	6	2711.2	15.71	
	7	2721.8	6.05	P
	8	2732.9 II	9.93	
	9	2756.5 II	10.18	
	10	2767.5		
	11	2799.7 II	14.98	
	12	2815.5 II	15.54	
	13	2824.4	8.13	
	14	2873.7 II	15.51	
	15	2896.5 II	15.54	
	16	2902.1 II	14.98	
	17	2929.4 II	9.93	
	18	2934.2 II	14.94	
	19	2938.6 II	14.98	
	20	3180.7 II	14.08	
	21	3247.6		
	22	3274.0		
R	23	3280.7	3.78	P
	24			
	25	3382.9	3.66	P

Table VI H - Cu

Self Reversed Lines	Plate Identification Number	Wavelength (Å)	Excitation Energy (ev)	Lines Present in Cu Arc Spectrum
	1	2590.5 II	10.93	
	2	2598.8 II	10.7	
	3	2600.3 II	10.96	
	4	2618.4	6.12	P
	6	2689.3 II	10.7	
	7	2701.0 II	10.96	
	8	2703.2 II	10.93	
	9	2713.5 II	10.70	
	10	2718.8 II	10.96	
	11	2766.4	.6.12	P
	12	2768.9	9.55	
	13	2824.4	5.78	P
	14	2882.9		P
	15	2961.2	5.57	P
	16	2997.4	5.78	P
	17	3010.8	5.50	P
	18	3036.1	5.72	P
	19	3063.4	5.69	P
	20	3073.8	5.42	
	21	3094.0	5.40	P
	22	3099.9	8.83	
	23	3108.6	8.82	
	24	3126.1	8.80	
	25	3128.7	8.93	
	26	3140.3	8.78	
	27	3142.4	8.92	
	28	3146.8	8.91	
	29	3194.1	5.52	P
	30	3208.2	5.50	P
	31	3223.4	9.09	
	32	3224.7	9.09	
	33	3231.2	8.94	
	34	3235.7	9.07	
	35	3243.2	8.92	
R	36	3247.5	3.82	P

Table VI H -Cu Continued

	37	3266.0	9.37	
	38	3268.3	8.94	
R	39	3274.0	3.78	P
	40	3280.0	5.42	P
	41	3282.7	8.93	
	42	3290.5	8.84	
	43	3292.8	5.15	
	44	3307.0		
	45	3317.0		
	46	3319.0		
	47	3335.0		
	48	3349.0		
	49	3365.0		
	50	3381.0		

Table VI I - Au

Self Reversed Lines	Plate Identification Number	Wavelength (Å)	Excitation Energy (ev)	Lines Present in Cu Arc Spectrum
	1	2590.0		P
	2	2641.5		P
R	3	2676.0	4.63	P
	4	2688.7		P
	5	2700.9		P
	6	2748.3		P
	7	2802.2		
	8	2820.0		
	9	2822.7		
	10	2825.5		
	11	2883.5		P
	12	2892.0		
	13	2905.9 I + II		
	14	2907.1		
	15	2913.5 II		
	16	2932.2 I + II		
	17	2954.4		
	18	2990.3 II		
	19	2995.0 II		
	20	3029.2		P
	21	3033.2		
R	22	3122.8	5.10	P
	23	3204.7		
	24	3230.6 I + II		
	25	3247.5 Cu		
	26	3274.0 Cu		

Table VI J - Zn

Self Reversed Lines	Plate Identification Number	Wavelength (Å)	Excitation Energy (ev)	Lines Present in Cu Arc Spectrum
	1	2558.0 II	10.95	
	2	2756.5	8.50	P
	3	2771.0	8.50	P
	4	2800.9 I + II	8.50	P
	5	3018.4	8.11	
	6	3035.8	8.11	
	7	3072.1	8.11	P
	8	3075.9	4.03	P
R	9	3282.3	7.78	P
R	10	3302.6	7.78	P
R	11	3345.6	7.78	P

Table VI K - Ge

Self Reversed Lines	Plate Identification Number	Wavelength (Å)	Excitation Energy (ev)	Lines Present in Cu arc Spectrum
	1	2589.2		P
R	2	2592.5		P
R	2A	2644.2		P
R	3	2651.2 (0.6)		P
R	4	2691.3		P
R	5	2709.6		P
	6	2740.4		P
R	7	2754.6		P
	8	2793.9		P
	9	2802.0		
	10	2829.0		P
	11	2845.5 II		
R	12	3039.1	4.38	P
	13	3129.8	4.84	P
	14	3247.5 Cu		
R	15	3269.5	4.67	P
	16	3274.0 Cu		

Table VI L - Si

Self Reversed Lines	Plate Identification Number	Wavelength (Å)	Excitation Energy (ev)	Lines Present in Cu Arc Spectrum
	1	2631.3	6.62	P
	2	2881.6	5.08	P
R	3	2987.7	4.93	P
	4	3086.4 III	21.72	
	5	3093.3 III	21.71	

Table VII

Change in Intensity with Increasing Joule Output

Relative Intensity

Joules Out	Single Pulse Laser Beam (No Interaction)	Multiple Pulse Laser Beam (Interaction)
0.12	1.00	1.00
0.30	2.29	2.32
0.54	4.00	4.26
0.65	4.91	5.25

Table VIII

Calibration Curve for a 1030 Plate Emulsion from 2600-3300Å

A. Excitation Conditions for Baird 3.0 Meter Eagle Spectrograph with DC Arc Stand

      250 volts

        3 amper Fe arc

      25 micron slit width

      10 mm slit height

       6 second exposure

       4 step sector (ratio of steps = 1.585:1)

B. Development Conditions

      5 minute development at 20°C using Eastman D-19 developer

     30 second shot stop in 5% acetic acid

      5 minute fixing at 20°C using Eastman Kodak fixing solution

C. Emulsion Calibration Curve (Figure 10)

      Transmittance values are obtained form the scatter diagram and plotted against relative intensity on log-log graph paper. The following is the data used for constructing the calibration curve for a 1030 emulsion.

Table X

Quantitative Analysis of Aluminum Alloys Using AC Spark Source

A. Excitation Conditions for Baird 3.0 Meter Eagle Spectrograph with AC Spark Stand

        250 volts
       2750 volt peak power
          3 breaks per half cycle
          3 mm analytical gap
         10 second prespark
     6 - 8 second spark exposure
         25 micron slit width
        2.5 mm slit height
     Capacitance - 0.005 uf
     Inductance - 44 uh
     RF Current - 7.5 amps

B. Development Conditions

    Development conditions are similar to those described in Table X.

C. Working Curves (Figure 12)

    The working curves are constructed by plotting the relative intensity ratio of a selected element spectrum line and a matrix line of equivalent characteristics versus element concentration on a log-log basis. The relative intensity values represent the mean value of six different exposures. The 3059.4 Al emission line is used as an internal standard. Transmittance values for this line range from 15 to 40%. The following is the data used in constructing the working the curves:

Table X A - Cu(3247.5Å)

Series	Sample	Average I(Cu)/I(Al)	Conc.(%)
2S	SS-2-C	3.28	0.17
	SS-11	1.26	0.044
	SA-665-C	3.88	0.21
3S	SS-3-E	2.93	0.15
	SA-808-29	2.08	0.084
	SA-811-7	3.80	0.24

Table X B - Si(2881.6Å)

Series	Sample	Average I(Si)/(Al)	Conc. (%)
2S	SS-2-C	o.512	0.17
	SS-1-1	0.418	0.12
	SA-665-C	0.281	0.07
3S	SS-3E	0.638	0.26
	SA-808-29	0.351	0.10
	SA-811-7	0.928	0.46
11S	SS-11-DB	0.915	0.28
	SA-459	0.349	0.07
	SA-460-5	1.73	0.63
24S	SS-24-B	0.551	0.16
	SA-754-1	0.758	0.24
	SA-755-B	1.05	0.42
75S	SS-75-J	0.837	0.27
	SA-789-F	0.712	0.21
	SA-767-T	0.943	0.32

Table X C - Mg(2852.1Å)

Series	Sample	Average I(Mg)/I(Al)	Conc. (%)
2S	SS-2-C	0.904	0.029
	SS-1-1[1]	0.109	0.0015
3S	SS-3-E	0.718	0.026
	SA-808-29[1]	0.115	0.002
	SA-811-7	1.20	0.052
11S	SS-11-DE	0.979	0.037
	SA-459-5	0.506	0.02
	SA-460-5	1.04	0.04

1 14 second exposure

Table X D - Fe(2755.7Å)

Series	Sample	Average I(Fe)/I(Al)	Conc. (%)
2S	SS-2-C	1.25	0.40
	SS-1-1	0.993	0.30
	SA-665-C	1.34	0.45
3S	SS-3-E	1.27	0.49
	SA-808-29	0.861	0.26
	SA-811-7	1.80	0.76
11S	SS-11-DB	1.73	0.47
	SA-459-5	0.948	0.24
	SA-460-5	2.12	0.57
24S	SS-24-B	1.04	0.29
	SA-754-1	0.615	0.14
	SA-755-B	1.56	0.49
75S	SS-75-J	0.944	0.23
	SS-789-F	1.09	0.26
	SA-767-T	2.00	0.53

Table X E – Mn(2933.1Å)

Series	Sample	Average I(Mn)/I(Al)	Conc. (%)
2S	SS-2-C	0.341	0.041
	SS-1-1	--	0.004
	SA-665-C	0.273	0.030
11S	SS-11-DB	0.408	0.049
	SA-459-5	0.356	0.04
	SA-160-5	0.507	0.07
24S	SS-24-B	4.73	0.68
	SA-754-1	3.51	0.48
	SA-755-B	6.79	0.90
75S	SS-75-J	1.19	0.16
	SS-789-F	1.13	0.14
	SA-767-T	1.77	0.28

Table XI

Quantitative Analysis of Aluminum Alloys Using Laser Microprobe

A. Excitation Conditions for Jarrell Ash F/6.3 Spectrograph
    with Laser Unit

        Laser setting - 10
        Lens setting - 10
        Grating setting - 2000 (2630 - 3300Å)
        50 micron slit width
        4 mm slit height
        6 superimposed laser shots

B. Development Conditions

    Development conditions are similar to those described
    in Table X

C. Working curves (Figure 12)

    Method is similar to that described for A. C. spark.
The relative intensity values represent the mean value of four
different exposures. The 3050.0 Al emission line is used as
an internal standard. The large background around the 3059.4
line prevents its use as an internal standard. Transmittance
values for the internal standard line range from 26 - 40%.
The following is the data used in constructing the working curves:

Table XIII A - Cu(3247.5Å)

Series	Sample	Average I(Cu)/I(Al)	Conc. (%)
2S	SA-665-C	0.699	0.21
	SS-11	0.381	0.044
	SS-2-C	0.638	0.17
3S	SA-808-29	0.488	0.084
	SA-811-7	0.739	0.24
	SS-3-E	0.612	0.15

Table XI B - Si(2881.6)

Series	Sample	Average I(Si)/I(Al)	Conc. (%)
3S	SA-811-7	0.451	0.46
	SS-3-E	0.388	0.26
11S	SS-11-DB	0.397	0.28
	SA-460-5	0.490	0.63
24S	SA-754-1	0.379	0.24
	SA-755-B	0.434	0.42
75S	SS-75-J	0.391	0.27
	SA-767-T	0.415	0.32

Table XI C - Mg(2852.1)

Series	Sample	Average I(Mg)/I(Al)	Conc. (%)
2S	SS-2-C	0.527	0.029
3S	SA-811-7	0.683	0.052
	SS-3-E	0.492	0.026
11S	SS-11-D	0.581	0.037
	SA-459-5	0.438	0.02
	SA-460-5	0.594	0.04

Table **XII**

Precision of Analysis for an Aluminum Alloy[1]

Impurity	Emission Line	Impurity Conc. (%)	Coefficient of Variation	
			AC SPark	0.7 Joule Laser[2]
Cu	3247	0.24	3.75	13.3
Mn	2933	1.55	2.23	8.52
Si	2881	0.46	3.84	30.0
Mg	2852	0.05	4.04	14.3
Fe	2756	0.76	2.35	10.6

1 Nine degrees of freedom

2 Six superimposed shots

Table XIII

Concentration of Iron Alloys

Low Alloy Steels (86-B-30-45)	% Cr	% Mo	% Mn	% Ni
L - 1	0.41	0.073	0.28	0.33
L - 2	0.53	0.09	0.35	0.39
L - 3	0.67	0.117	0.47	0.53
L - 5	1.11	0.203	0.83	0.97
L - 6	1.37	0.271	1.05	1.24
L - 7	1.71	0.365	1.43	1.67
L - 8	1.73	0.470	1.141	2.29

Cast Iron

	% Cr	% Mo	% Mn	% Ni
C - 3	0.0086	0.044	0.33	0.013
C - 4	0.031	0.101	0.33	0.032
C - 5	0.057	0.006	0.37	0.034
C - 6	0.242	0.025	0.48	0.071

12% Cr Steel

	% Cr	% Mo	% Mn	% Ni
Cr - 5			0.25	0.20
Cr - 10			0.70	0.74
Cr - 11		0.62	0.48	0.41

Tool Steel

	% Cr	% Mo	% Mn	% Ni
836			0.21	
837		1.84	0.48	
840	2.12	0.368	0.15	
841		1.44	0.27	

18% Cr, 12% Ni Steel

	% Cr	% Mo	% Mn	% Ni
329			0.54	2.05
1931			1.30	3.90
1967			1.37	1.93

Table XIV

Quantitative Analysis of Iron Alloys With a

0.12 Joule, Single Spike Laser Beam

A. Excitation conditions for Jarrell Ash F/6.3 Spectrograph with Laser
Unit.

Laser setting - 10

Lens setting - 10

Grating setting - 2500 (3320 - 4050Å)

50 micron slit width

4 mm slit height

20 superimposed laser shots

3250V fed to capacitor bank

B. Development Conditions

Development conditions are similar to those for emulsion
calibration curve.

C. Working Curves (Figure 13)

Method is similar to that described for AC spark. The
relative intensity values represent the mean values of four different
exposures. Emission and matrix lines suitable for quantitative
analysis are: Mn(4041.4/Fe(4014.5), Mo(3864.1)/Fe(3867.2),
Ni(3461.6)/Fe(3471.3), and Cr(3368.1)/Fe(3370.8). The following is
the data used in constructing working curves:

Table XIV A - Mn(4041.4)/Fe(4014.5)

Series	Sample	Average I(Mn)/I(Fe)	Conc.(%)
Low Alloy	L – 1	0.681	0.28
Steel	L – 2	0.736	0.35
	L – 3	0.847	0.47
	L – 5	1.14	0.83
	L – 6	1.32	1.05
	L – 7	1.48	1.42
	L – 8	1.48	1.42
Cast Iron	C – 3	0.730	0.33
	C – 4	0.730	0.33
	C – 5	0.738	0.37
	C – 6	0.923	0.48
12% Cr Steel	Cr – 5	0.621	0.25
	Cr – 10	1.02	0.70
	Cr – 11	0.920	0.48
Tool Steel	836	0.571	0.21
	837	0.902	0.48
	840	0.497	0.15
	841	0.672	0.27
18% Cr, 8% Ni	329	1.76	2.05
	1967	1.74	1.93
	1931	2.38	3.90

Table XIVB - Mo(3864.1)/Fe(3867.2)

Series	Sample	I(Mo)/I(Fe)	Conc. (%)
Low Alloy Steel	L - 1	0.461	0.073
	L - 2	0.507	0.09
	L - 3	0.552	0.117
	L - 5	0.718	0.203
	L - 6	0.838	0.271
	L - 7	0.921	0.365
	L - 8	1.07	0.470
Cast Iron	C - 3	0.348	0.044
	C - 4	0.519	0.101
	C - 5	0.399	0.060
	C - 6	0.262	0.025
12% Cr Steel	Cr - 5		
	Cr - 10		
	Cr -	1.22	0.62
Tool Steel	836		2.80
	837	1.85	1.50
	840	0.442	0.070
	841	1.44	0.84
18% Cr, 12% Ni	329	1.14	0.543
	1967	1.77	1.30
	1931	1.85	1.37

Table XIVC - Ni(3461.6)/Fe(3471.3)

Series	Sample	Average I(Ni)/I(Fe)	Conc.(%)
Low Alloy Steel	L-1	0.892	0.35
	L-2	0.918	0.39
	L-3	1.10	0.53
	L-5	1.37	0.77
	L-6	1.50	1.25
	L-7	1.81	1.68
	L-8	1.95	2.29
12% Cr Steel	Cr-5	0.713	0.20
	Cr-10	1.24	0.74
	Cr-11	1.02	0.41

Table XIVD - Cr(3368.1)/Fe(3370.8)

Series	Sample	Average I(Cr)/I(Fe)	Conc.(%)
Low Alloy Steel	L-1	0.447	0.41
	L-2	0.547	0.53
	L-3	0.619	0.67
	L-5	0.864	1.11
	L-6	0.991	1.37
	L-7	1.11	1.71
	L-8	1.13	1.73
Cast Iron	C-6	0.324	0.242
Tool Steel	840	1.27	2.12

Table XIVD - Fe(2755.7)

Series	Samples	Average I(Fe)/I(Al)	Conc. (%)
2S	SS-2-C	0.448	0.40
	SS-11	0.367	0.30
	SA-665-C	0.472	0.45
ΙS	SS-Ι-E	0.498	0.49
	SA-808-29	0.555	0.26
	SA-811-7	0.616	0.76
11S	SS-11-DB	0.490	0.47
	SA-459-5	0.557	0.24
	SA-460-5	0.538	0.57
24S	SS-24-B	0.368	0.29
	SA-755-B	0.505	0.49
75S	SS-75-J	0.524	0.23
	SA-789-F	0.552	0.26
	SA-767-T	0.514	0.53

Table XIVE - Mn(2949.2)

Series	Sample	Average I(Mn)/I(Al)	Conc. (%)
ΙS	SA-811-7	1.67	1.55
	SS-Ι-E	1.42	1.12
	SA-808-29	1.31	0.95
24S	SS-24-B	1.04	0.68
	SA-754-1	0.81	0.48
	SA-755-B	1.28	0.90
75S	SS-75-J	0.456	0.16
	SA-789-F	0.490	0.14
	SA-767-T	0.589	0.28

Table XV

Quantitative Analysis of Iron Alloys With a 0.65 Joule, Multiple Spike

Laser Beam

Procedures and conditions are similar to those described in Table XVI, except that 3600V is fed to capacitor bank instead of 3250V, and 3 laser shots are superimposed instead of 20.

Table XVA - Mn(4041.4)/Fe(4014.5)

Series	Sample	Average I(Mn)/I(Fe)	Conc.(%)
Low Alloy	L - 1	0.577	0.28
Steel	L - 2	0.681	0.35
	L - 3	0.75.	0.47
	L - 5	1.00	0.83
	L - 6	1.18	1.05
	L - 7	1.42	1.42
	L - 8	1.41	1.42
Cast Iron	C - 3	0.641	0.3.
	C - 4	0.641	0.33
	C - 5	0.661	0.37
	C - 6	0.819	0.48
12% Cr	Cr-5	0.517	0.25
Steel	Cr-10	0.947	0.70
	Cr-11	0.811	0.48
Tool	836	0.504	0.21
Steel	837	0.795	0.48
	840	0.412	0.15
	841	0.570	0.27
18% Cr,	329	1.81	2.05
8% Ni	1967	1.74	1.93

Table XVB - Mo(3864.1)/Fe(3867.2)

Series	Sample	I(Mo)/I(Fe)	Conc. (%)
Low Alloy Steel	L - 1	0.381	0.073
	L - 2	0.445	0.09
	L - 3	0.485	0.117
	L - 5	0.618	0.203
	L - 6	0.802	0.271
	L - 7	0.883	0.365
	L - 8	0.976	0.470
Cast Iron	C - 3	0.275	0.044
	C - 4	0.454	0.101
	C - 5	0.358	0.060
	C - 6	0.225	0.025
12% Cr Steel	Cr - 5		
	Cr - 10		
	Cr -	1.16	0.62
Tool Steel	836		2.80
	837	1.84	1.50
	840	0.368	0.070
	841	1.44	0.84
18% Cr, 12% Ni	329	1.04	0.543
	1967	1.67	1.30
	1931	1.75	1.37

Table XV C - Ni(3461.6)/Fe(3471.3)

Series	Sample	Average I(Ni)/I(Fe)	Conc. (%)
Low Alloy Steel	L - 1	0.845	0.33
	L - 2	0.917	0.39
	L - 3	1.05	0.53
	L - 5	1. 37	0.97
	L - 6	1.60	1.25
	L - 7	1.92	1.68
	L - 8	2.0`	2.29
12% Cr Steel	Cr - 5	0.667	0.20
	Cr - 10	1.32	0.74
	Cr - 11	1.00	0.41

Table XV D - Ni(3414.8)/Fe(3413.4)

Series	Sample	Average I(Ni)/I(Fe)	Conc. (%)
Low Alloy Steel	L - 1	0.529	0.33
	L - 2	0.617	0.39
	L - 3	0.646	0.53
	L - 5	0.790	0.97
	L - 6	0.871	1.25
	L - 7	0.945	1.68
	L - 8	1.039	2.29
Cast Iron	C - 3	0.249	0.0128
	C - 4	0.265	0.0317
	C - 5	0.334	0.034
	C - 6		0.071
12% Cr Steel	Cr - 5	0.472	0.20
	Cr - 10	0.726	0.74
	Cr - 11	0.653	0.41

Table XV E - Cr(3358.1),'Fe(3370.8)

Series	Sample	Average I(Cr)/I(Fe)	Conc. (%)
Low Alloy Steel	L - 1	0.342	0.41
	L - 2	0.399	0.53
	L - 3	0.472	0.67
	L - 5	0.725	1.11
	L - 6	0.832	1.37
	L - 7	1.05	1.71
	L - 8	1.02	1.73
Cast Iron	C - 6	0.225	0.242
Tool Steel	840	1.142	2.12

Table XV F - Cr(3593.5)/Fe(3594.6)

Series	Sample	Average I(Cr)/I(Fe)	Conc. (%)
Low Alloy Steel	L - 1	1.33	0.41
	L - 2	1.48	0.53
	L - 3	1.70	0.67
	L - 5	1.94	1.11
Cast Iron	C - 3		0.009
	C - 4	0.688	0.031
	C - 5	0.825	0.057
	C - 6	1.15	0.242

Table XVI

Precision of Analysis for an Iron Alloy[1]

Impurity	Emission Line	Impurity Conc.(%)	Coefficient of Variation	
			Single Spike[2] (0.12 Joule Output)	Multiple Spike[2] (0.65 Joule Output)
Mn	4041	1.05	6.45	9.3
Mo	3864	0.271	8.01	10.3
Ni	3462	1.25	8.26	12.2
Cr	3368	1.37	7.22	10.1

1   Nine degrees of freedom

2   Twenty superimposed laser shots

3   Three superimposed laser shots

Table XVII

Relative Intensity as Function of Laser Shots at a Fixed Joule Level

Joule Output	Superimposed Laser Shots	Mn(4041.4)/Fe(4041.5)			Mo(3864.1)/Fe(3867.2)		
		I(Mn)	I(Fe)	I(MN)/I(Fe)	I(MO)	I(Fe)	I(MO)/I(Fe)
0.12 (Single Pulse)	20	11.3	7.15	1.58	8.62	8.41	1.02
	16	9.23	6.02	1.53	7.11	6.88	1.03
	12	7.01	4.72	1.48	5.52	5.40	1.02
	8	5.22	3.48	1.50	4.10	4.02	1.02
0.65 (Multiple Pulse)	8	22.7	16.7	1.36	16.3	16.8	0.97
	6	17.5	12.0	1.46	12.7	13.0	0.98
	4	10.7	7.52	1.42	7.98	8.33	0.96
	3	8.88	6.14	1.44	6.84	6.92	0.99
	2	5.65	3.81	1.48	4.17	4.35	0.96

Joule Output	Superimposed Laser Shots	Ni(3461.6)/Fe(3471.3)			Cr(3368.1)/Fe(3370.8)		
		I(Ni)	I(Fe)	I(Ni)/I(Fe)	I(Cr)	I(Fe)	I(Cr)/I(Fe)
0.12 (Single Pulse)	20	11.9	6.10	1.95	10.2	9.23	1.11
	16	9.59	5.91	1.95	8.33	7.42	1.12
	12	7.80	3.71	2.10	6.58	5.98	1.10
	8	5.62	2.79	2.01	4.44	3.92	1.13
0.65 (Multiple Pulse)	8	23.2	11.5	2.02	22.9	20.5	1.11
	6	19.3	9.21	2.10	17.8	16.2	1.09
	4	12.7	6.22	2.04	11.2	10.5	1.07
	3	10.4	5.15	2.02	8.22	7.51	1.09
	2	6.69	3.33	2.01	5.23	4.88	1.07

Figure 1 Absorption spectrum of ruby
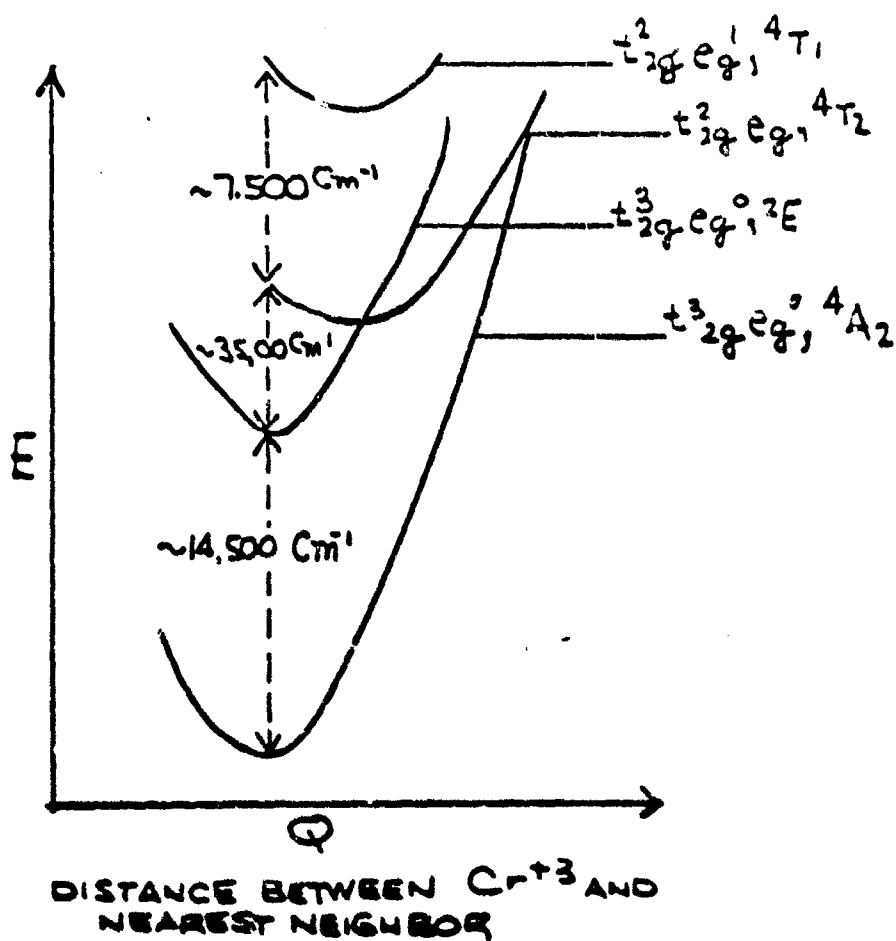
Figure 2 Energy level diagram for ruby
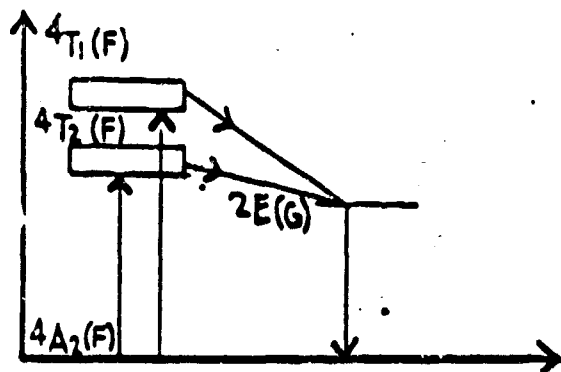
Figure 3 Laser action in ruby
Symbol in parenthesis is indicative
of the atomic state from which the
molecular level is derived.
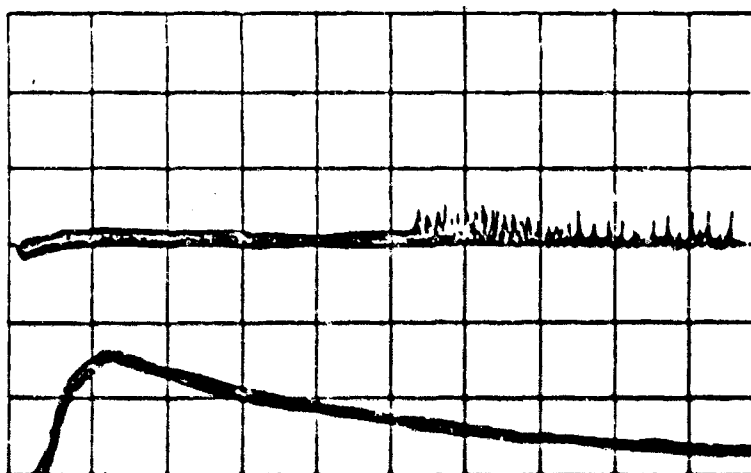
Figure 4   Intensity of radiation from ruby versus time.
Light emitted from ruby: upper trace.
Light emitted from flashlamp: lower trace.
       Horizontal scale = 1 cm = 0.1 milliseconds

LIGHT FILTER

PHOTO DETECTOR (See fig. 5C)

FUSED GLASS PLATES

ROTATING PRISM REFLECTOR

RUBY ROD

4% OF LASER LIGHT

96% OF LASER LIGHT

GLASS PRISM

55% REFLECTOR

XENON FLASHLAMP

EYE PIECE

HOUSING

F/6.3 SPECTROGRAPH (SEE fig 5B)

MICROSCOPE

SAMPLE VAPOR EXCITED TO LUMINESCENCE

SAMPLE

FOCUSING LENS
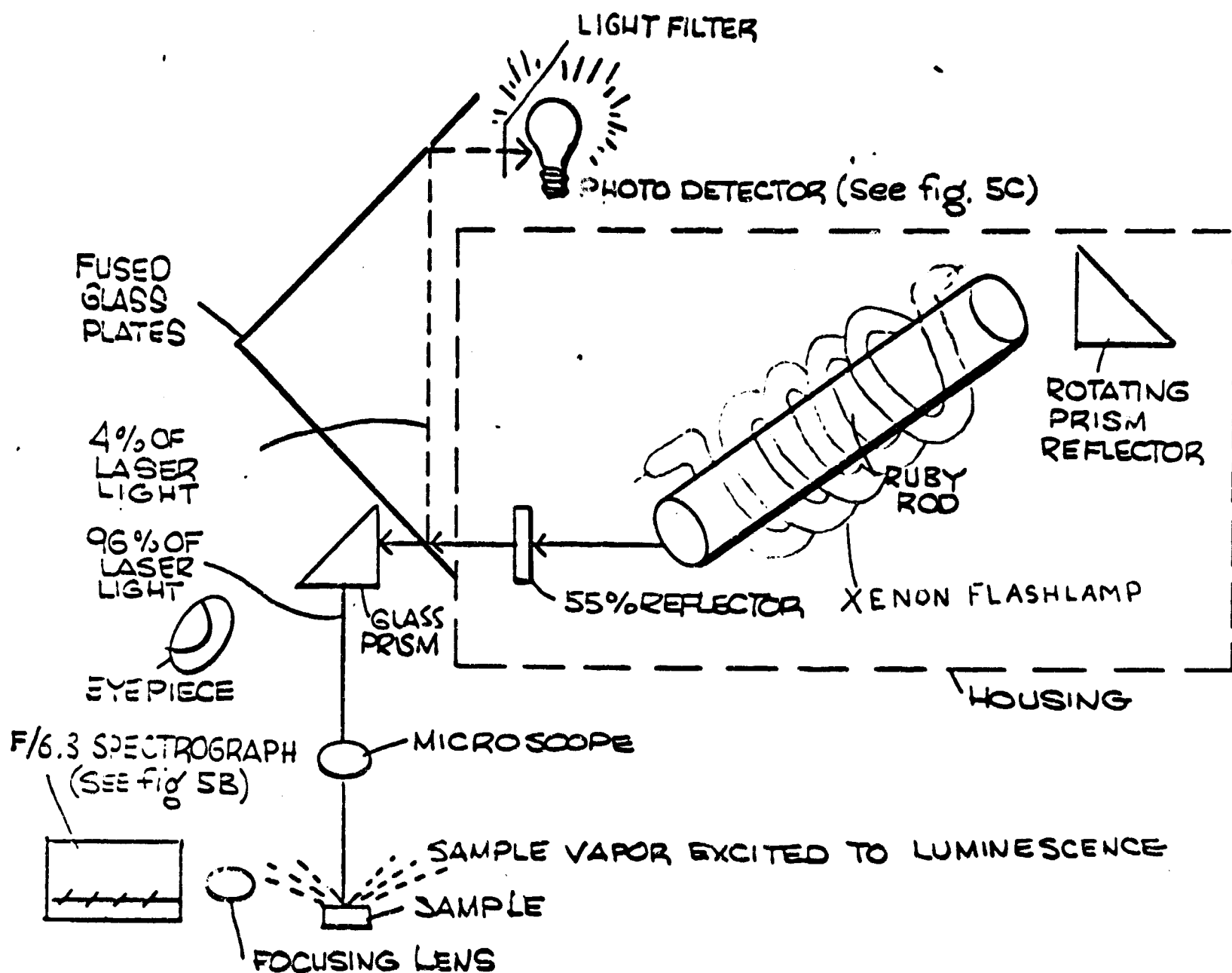
Figure 5A Laser Microprobe and monitoring system

PHOTOGRAPHIC PLATE

LARGE FOCAL MIRROR

GRATING

LARGE FOCAL MIRROR

ENTRANCE SLIT
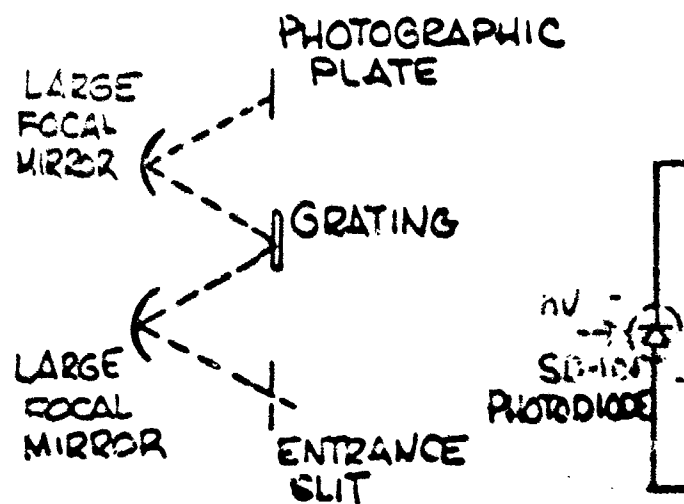
Figure 5B F/6.3 Spectrograph with Czerney-Turner mount

GROUND

90V

0.1 µF

hν

SD-100 PHOTODIODE

50 Ω

535 A OSCILLISCOPE

$RC = 3 \times 10^{-1}$ s
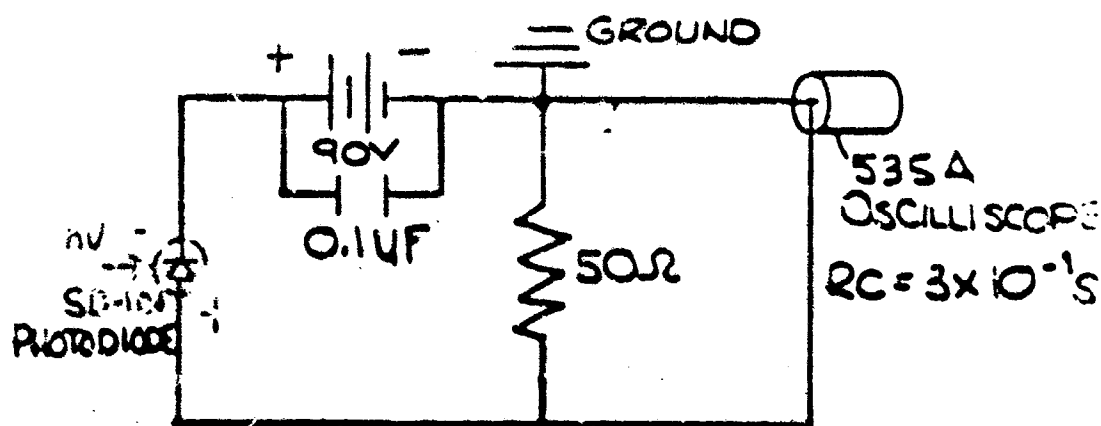
Figure 5C Electronic schematic of photodetector
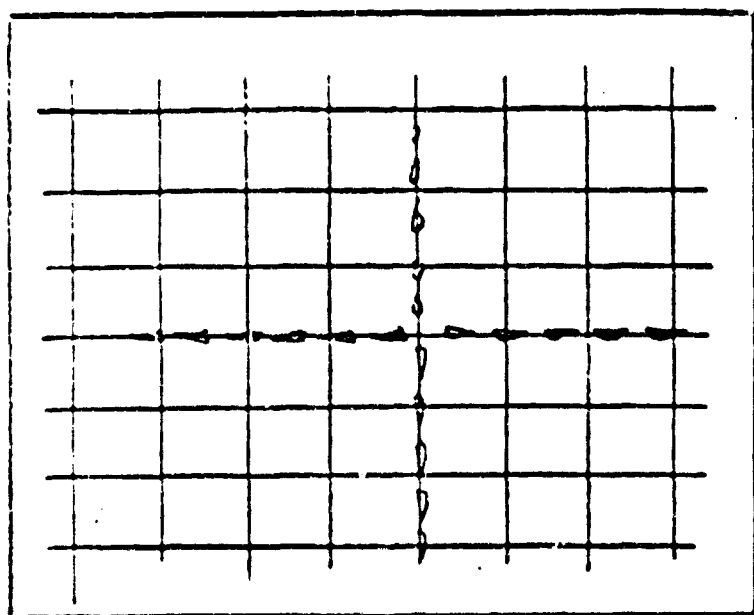
3050V
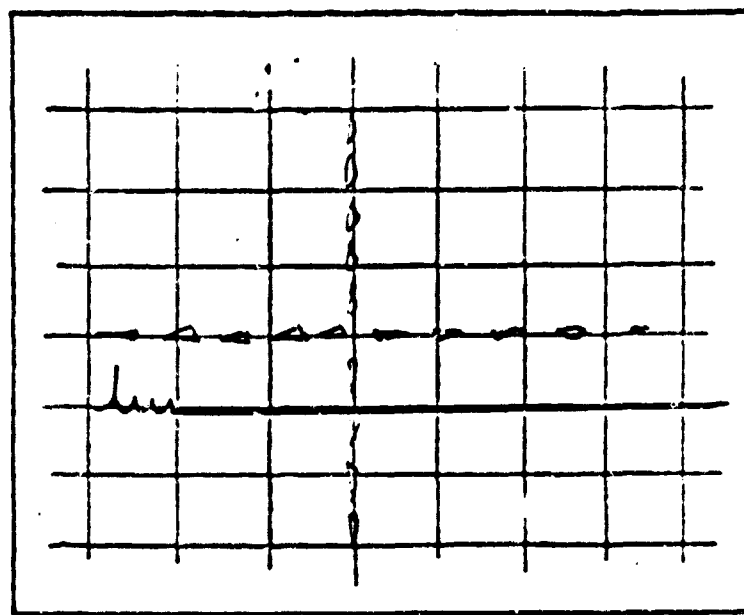
3100V
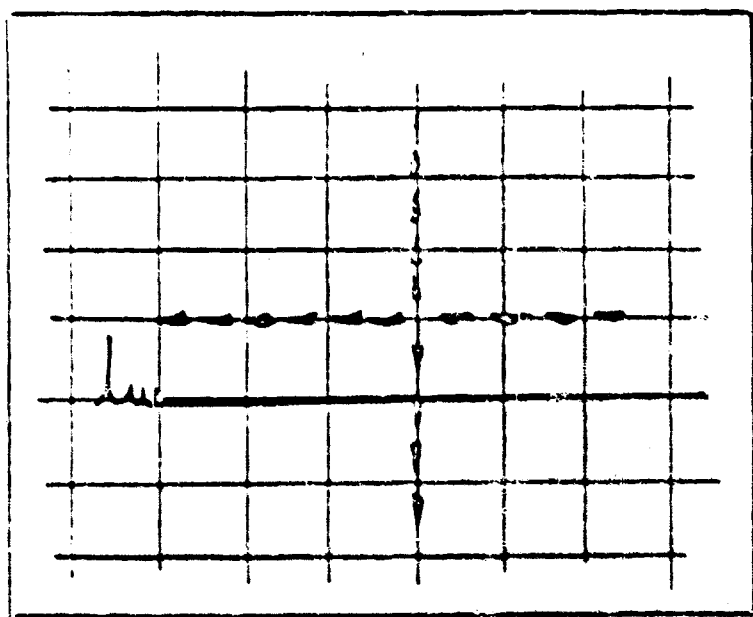
3150V
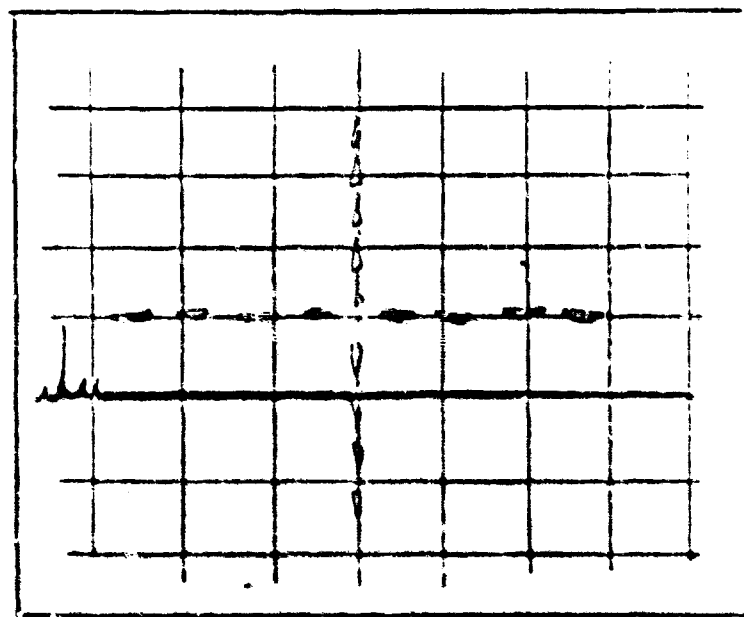
3200V

Figure 6   Change in laser pulse and power with increasing power input

Vertical scale   - 1 cm = 5 volts = 2 megawatts
Horizontal scale - 1 cm = 0.5 microseconds
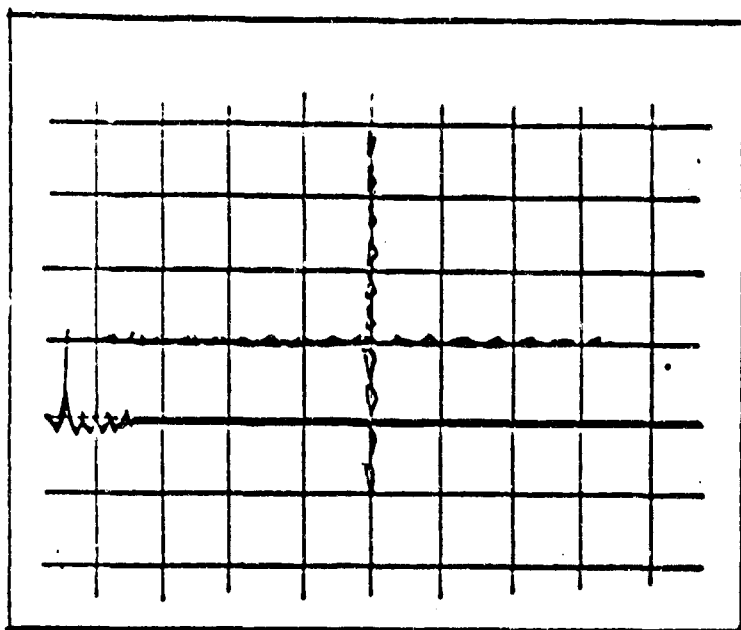
3250 V
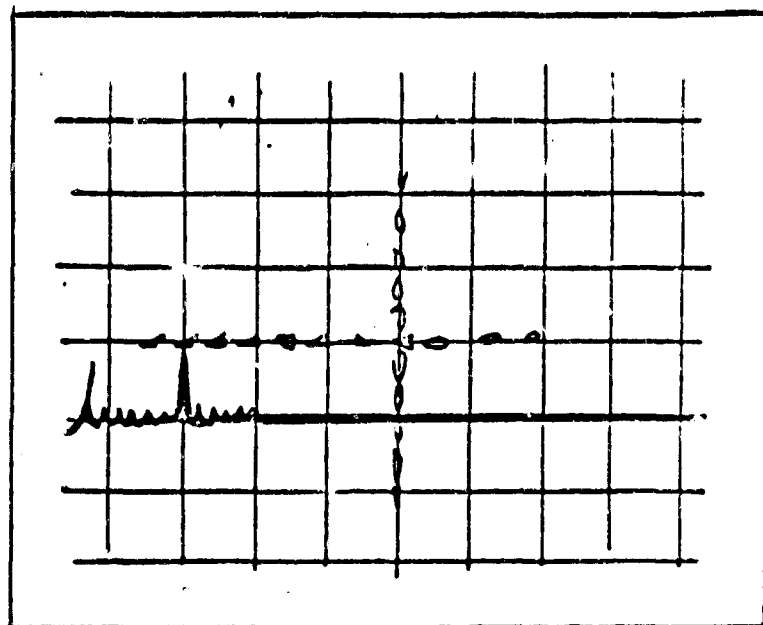
3350 V
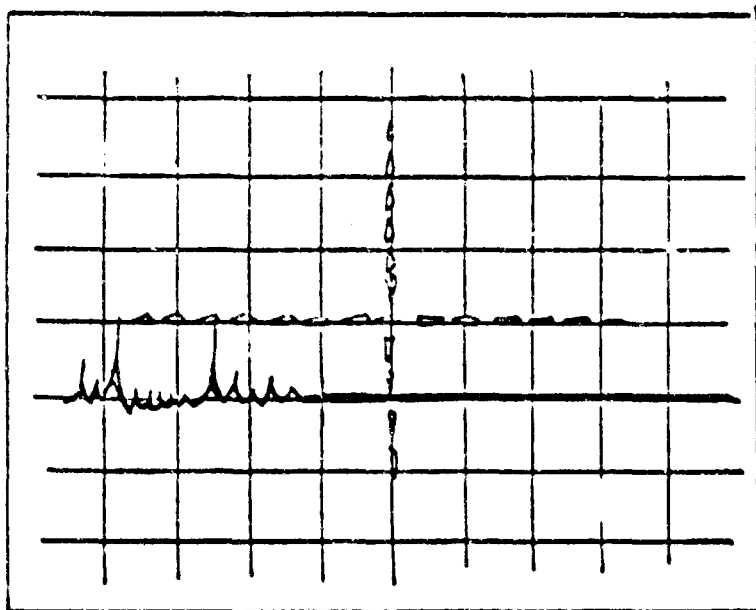
3480V
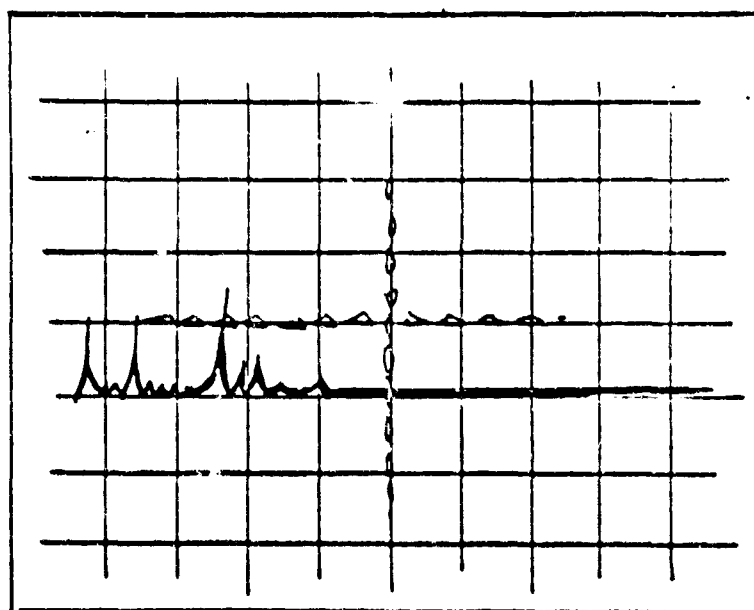
3600V

Figure 6 Continued

Vertical scale   - 1 cm = 5 volts = 2 megawatts
Horizontal scale - 1 cm = 0.5 microseconds

Figure 7   Craters produced by a 0.7 joule laser

Pb
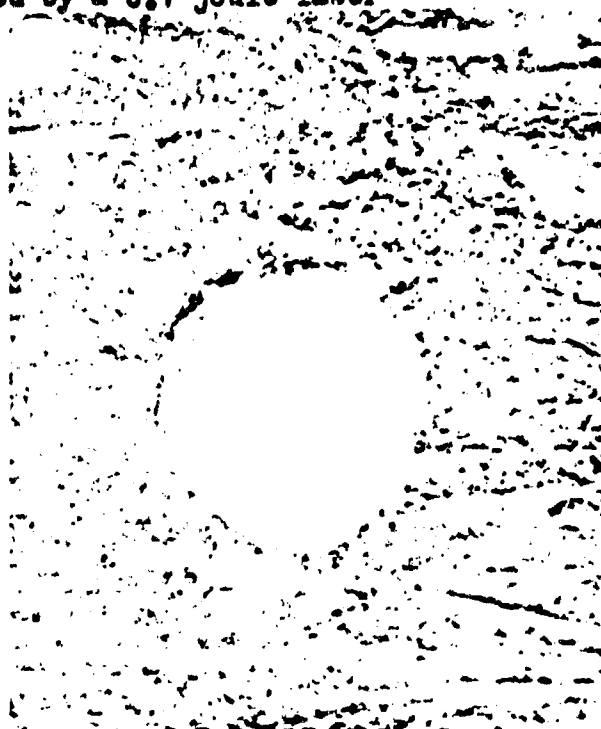
Sn

Al
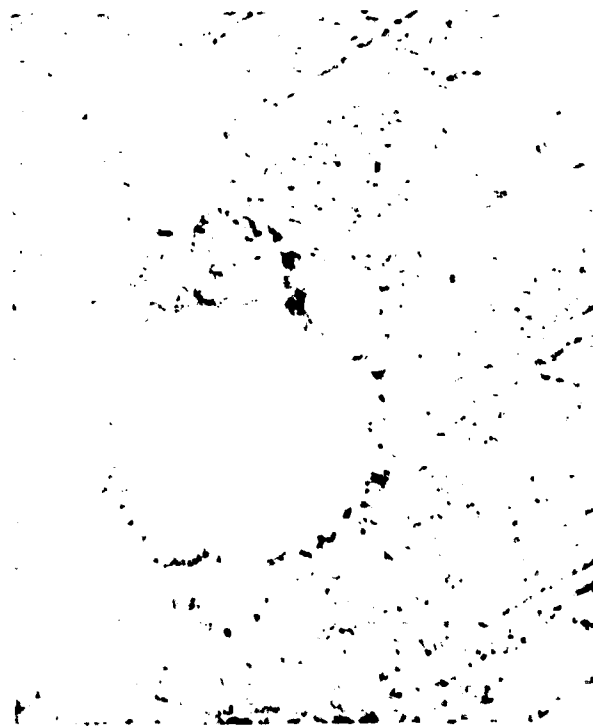
Cd
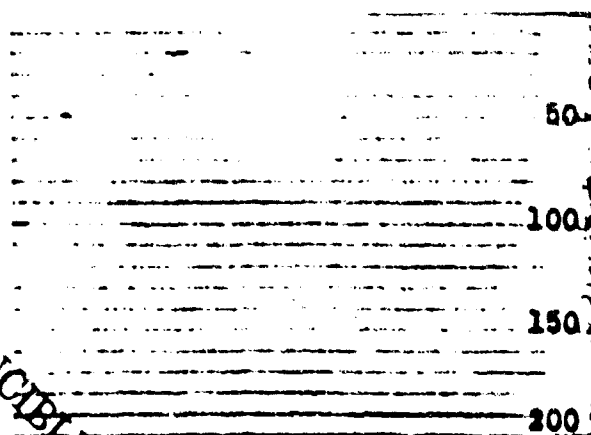
Diameter measuring
scale (microns)

50
100
150
200

Figure 7 Continued

Cu

Zn

Fe

Ta
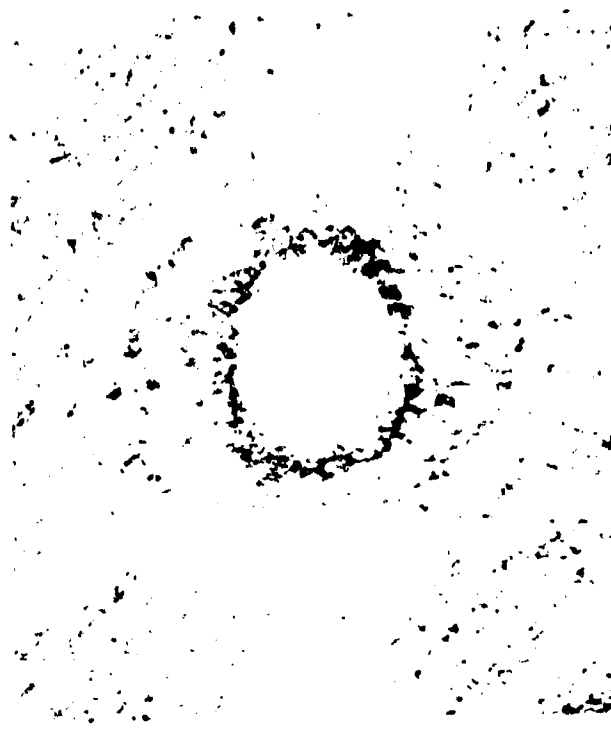
Figure 8 Emission lines produced by a 0.7 joule laser

Figure 8A

3385Å ... Figure 8A ... 2570Å

La 1
2
Pb 1
2
Sn 1
2
Al 1
2
Mg 1
2
Cd 1
2

3385Å ... Figure 8B ... 2570Å

Ag 1
2
Cu 1
2
Au 1
2
Zn 1
2
Ge 1
2
Si 1
2
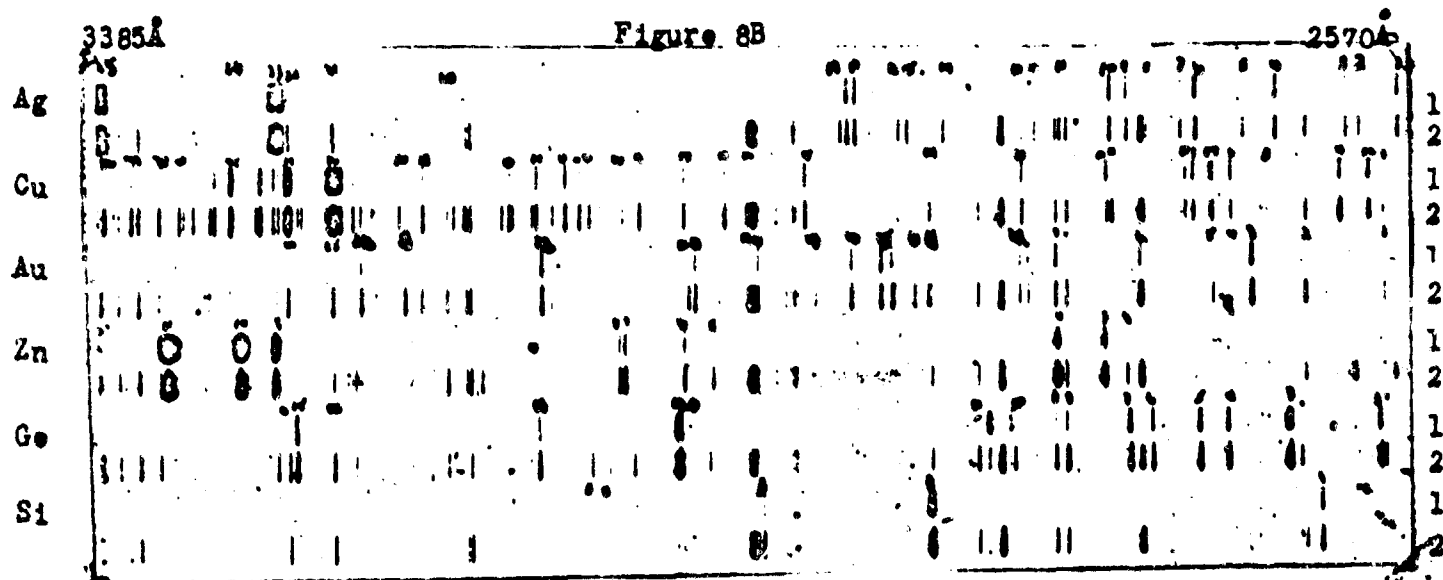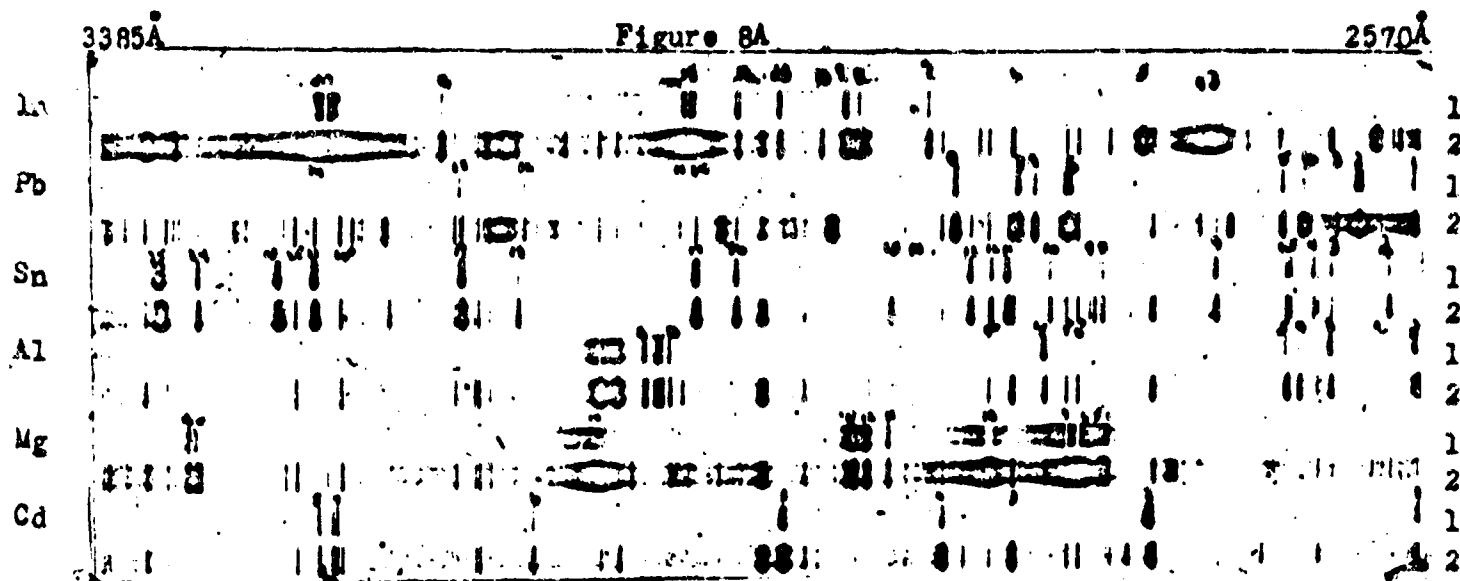
1 Without cross excitation

2 With cross excitation
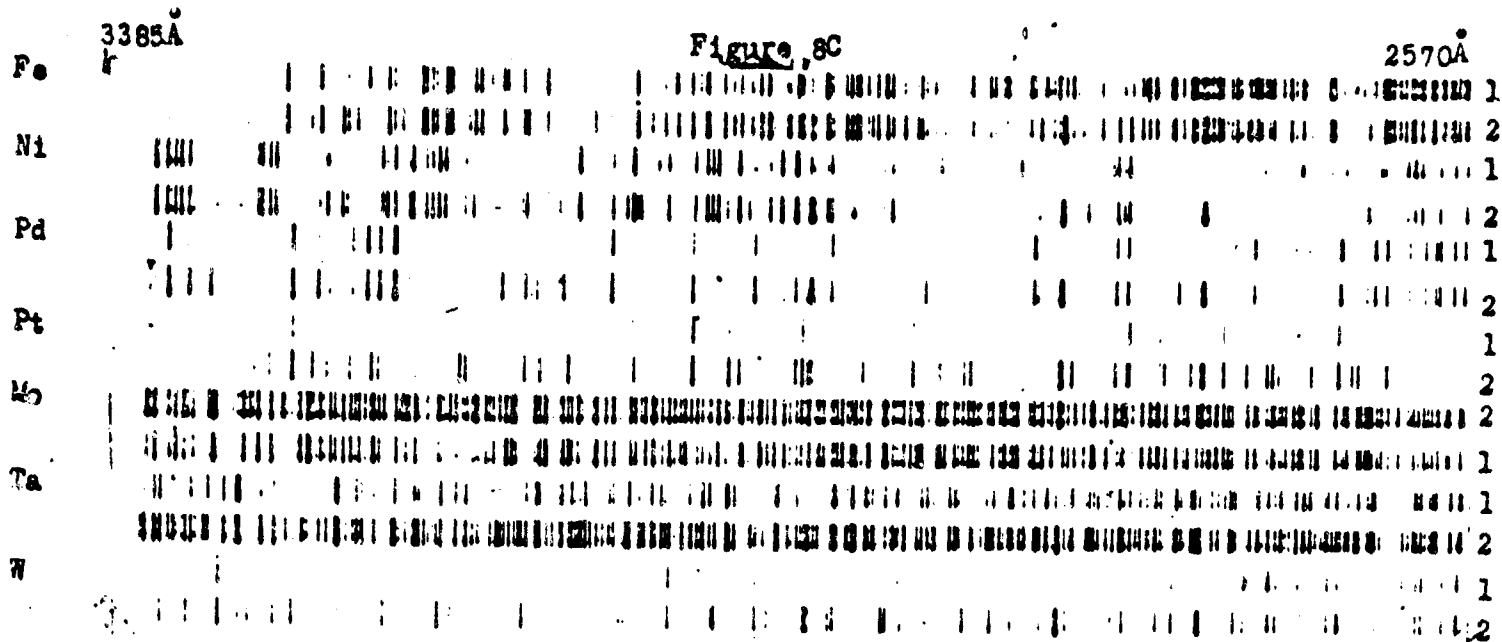
Figure 9 Quantitative analysis of iron alloys with a 0.7 joule laser
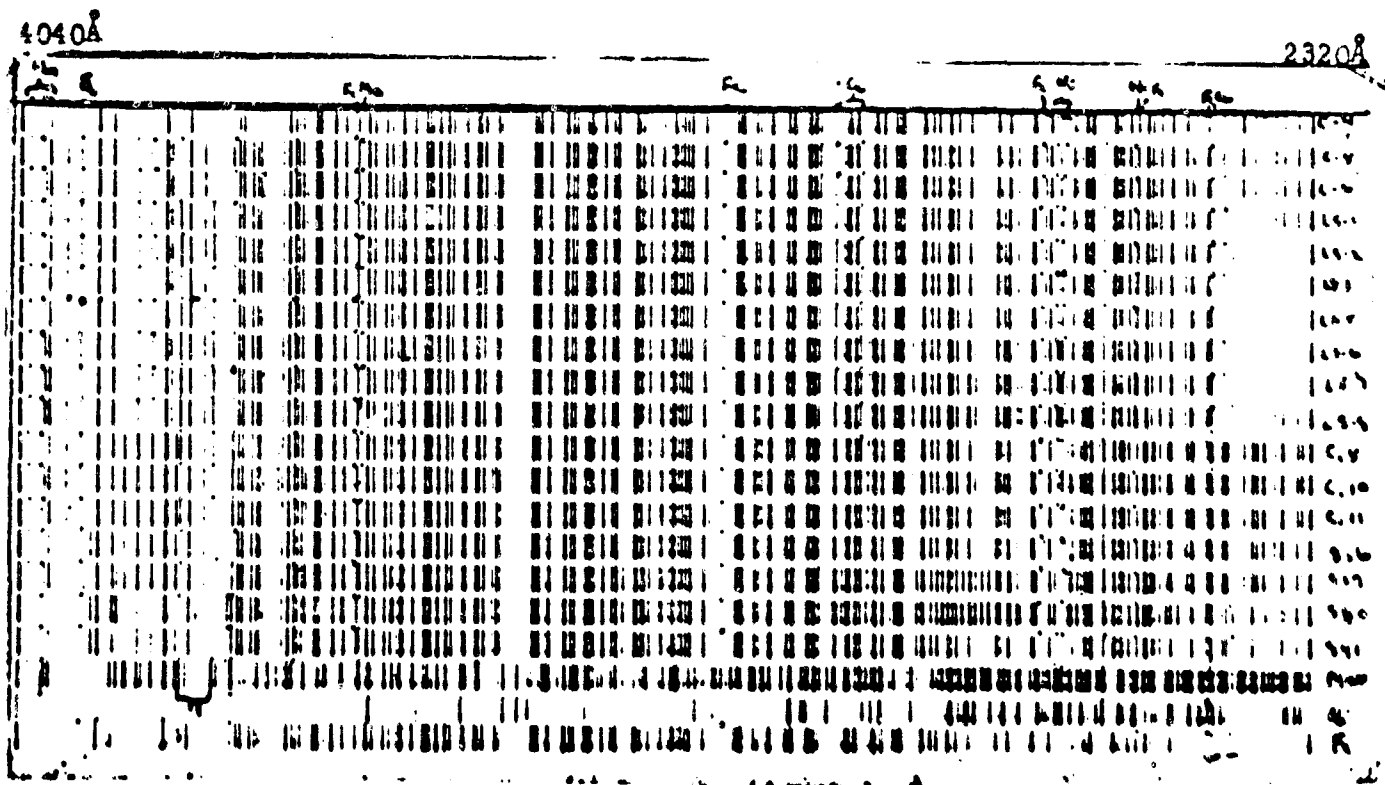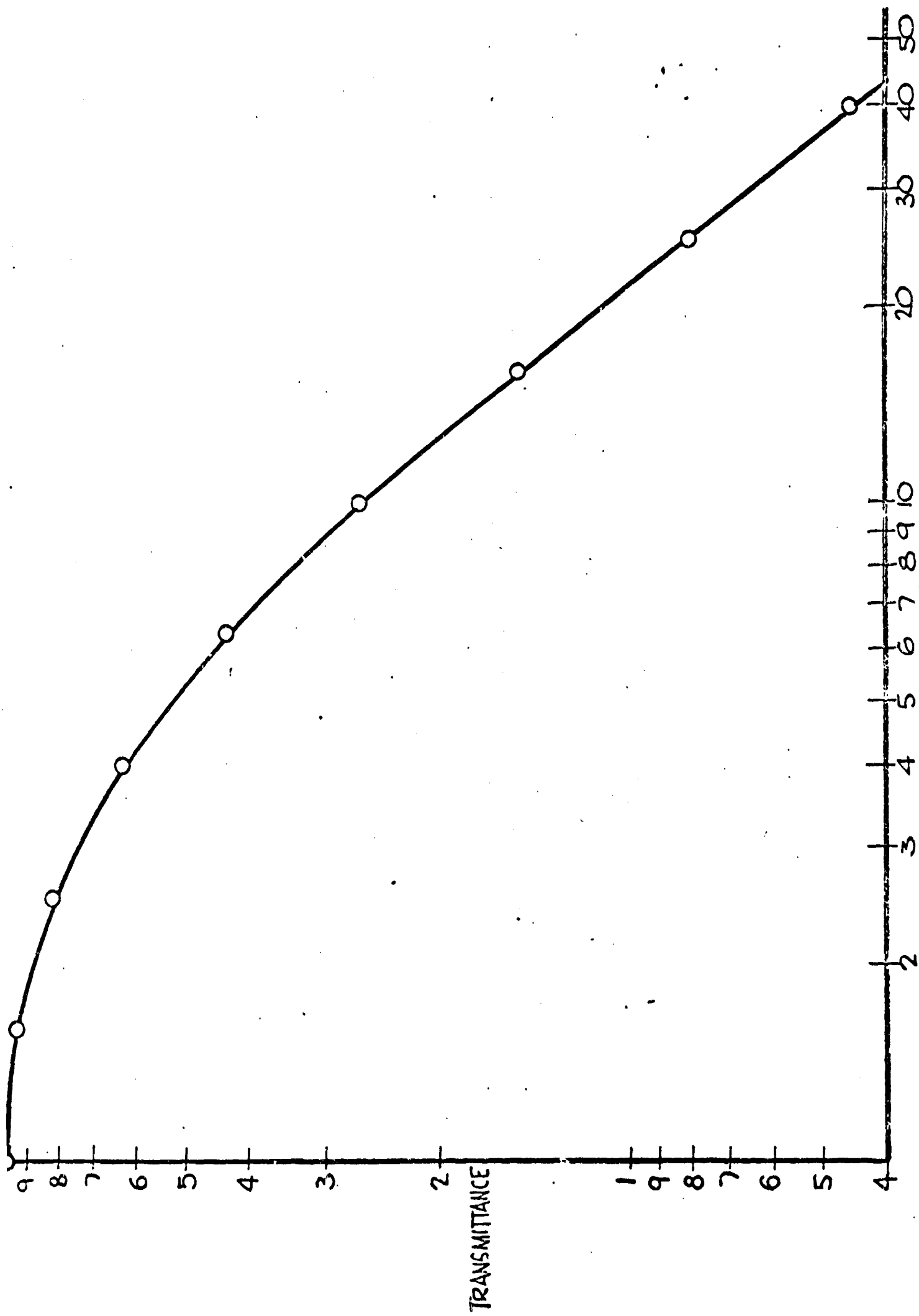
Figure 10 Calibration curve for a 1030 photographic emulsion
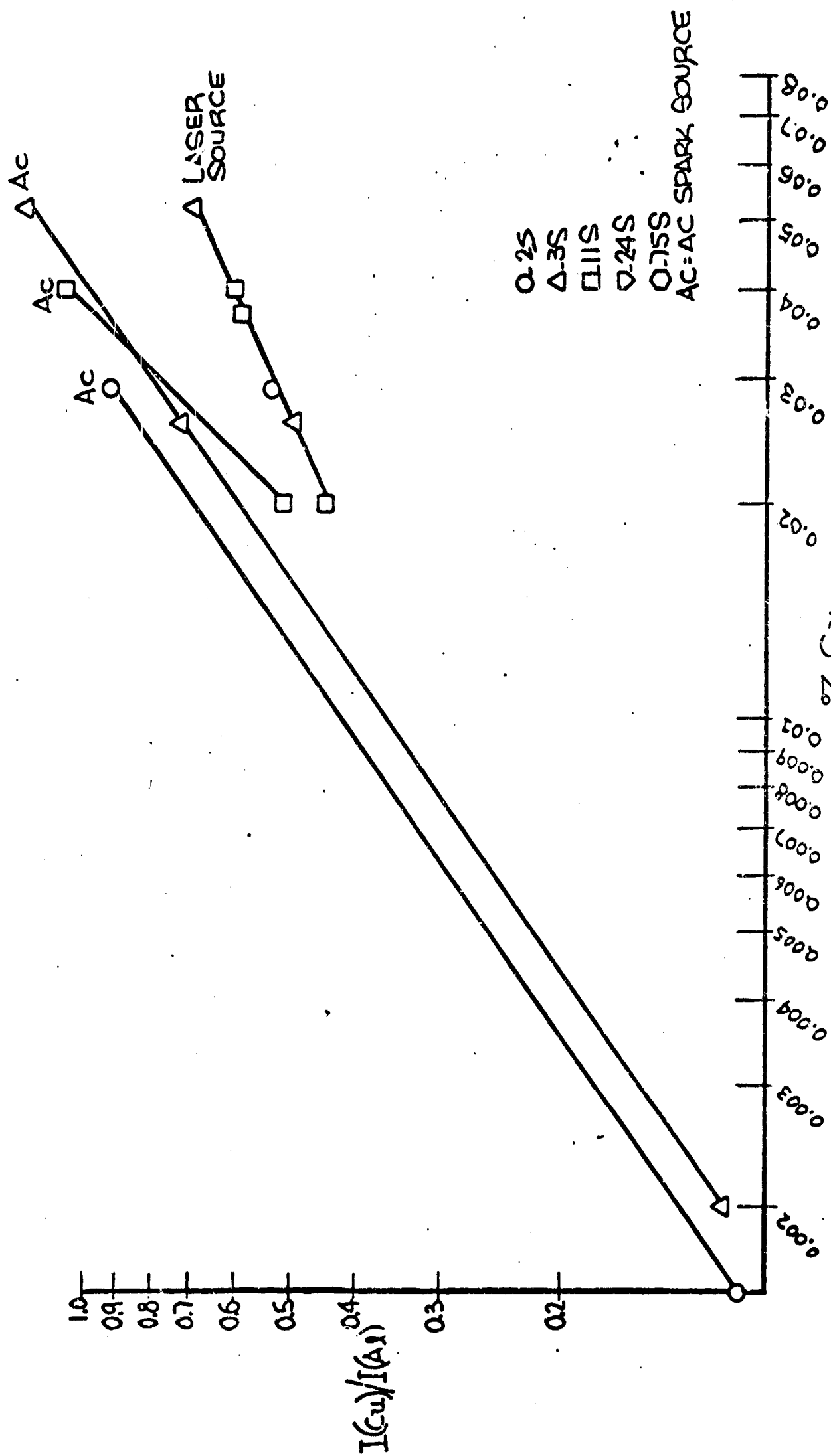
Figure 11A Quantitative analysis Cu in aluminum alloys with an AG spark and a laser excitation source
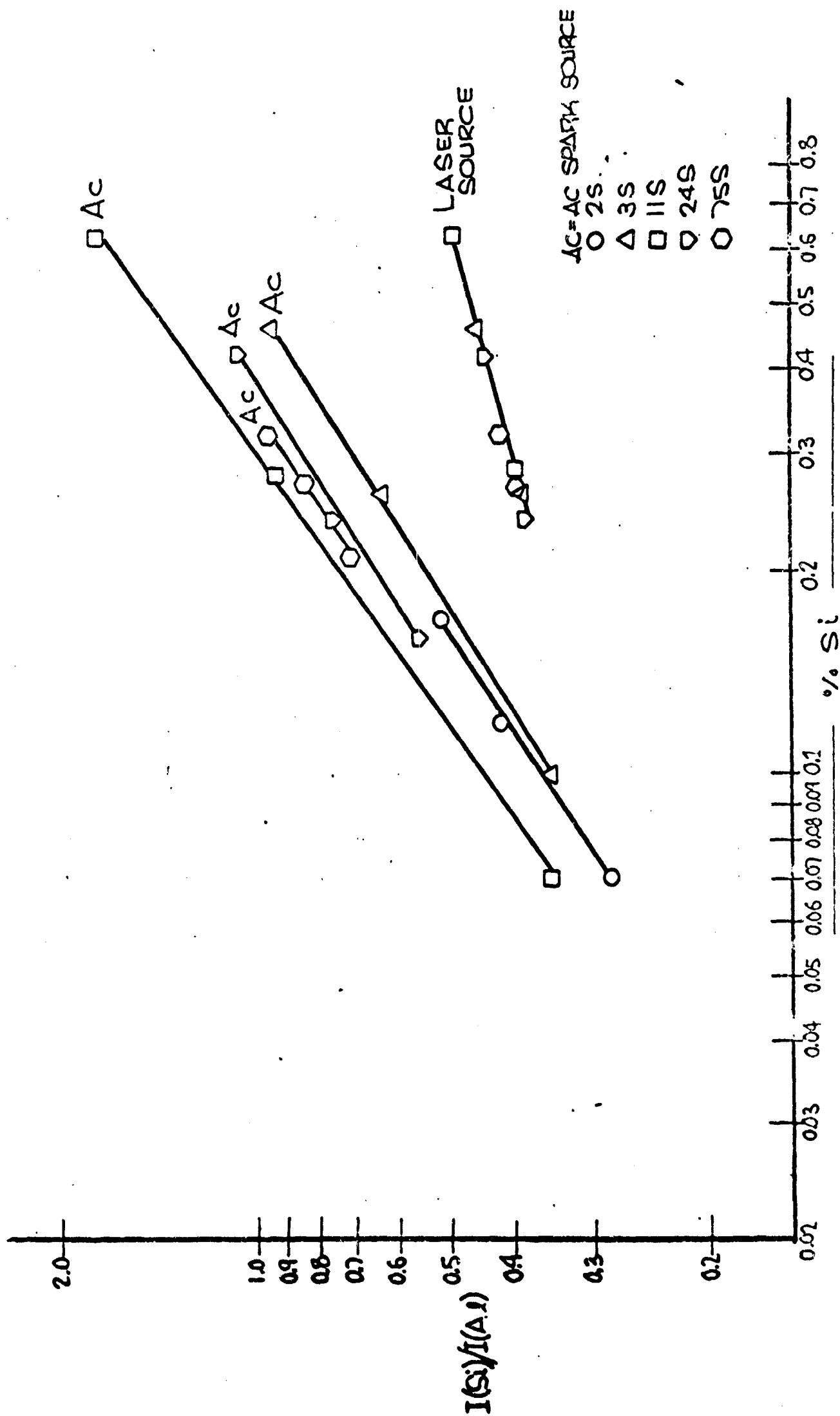
Figure 11B Quantitative analysis of Si in aluminum alloys with an AC spark and a laser excitation source
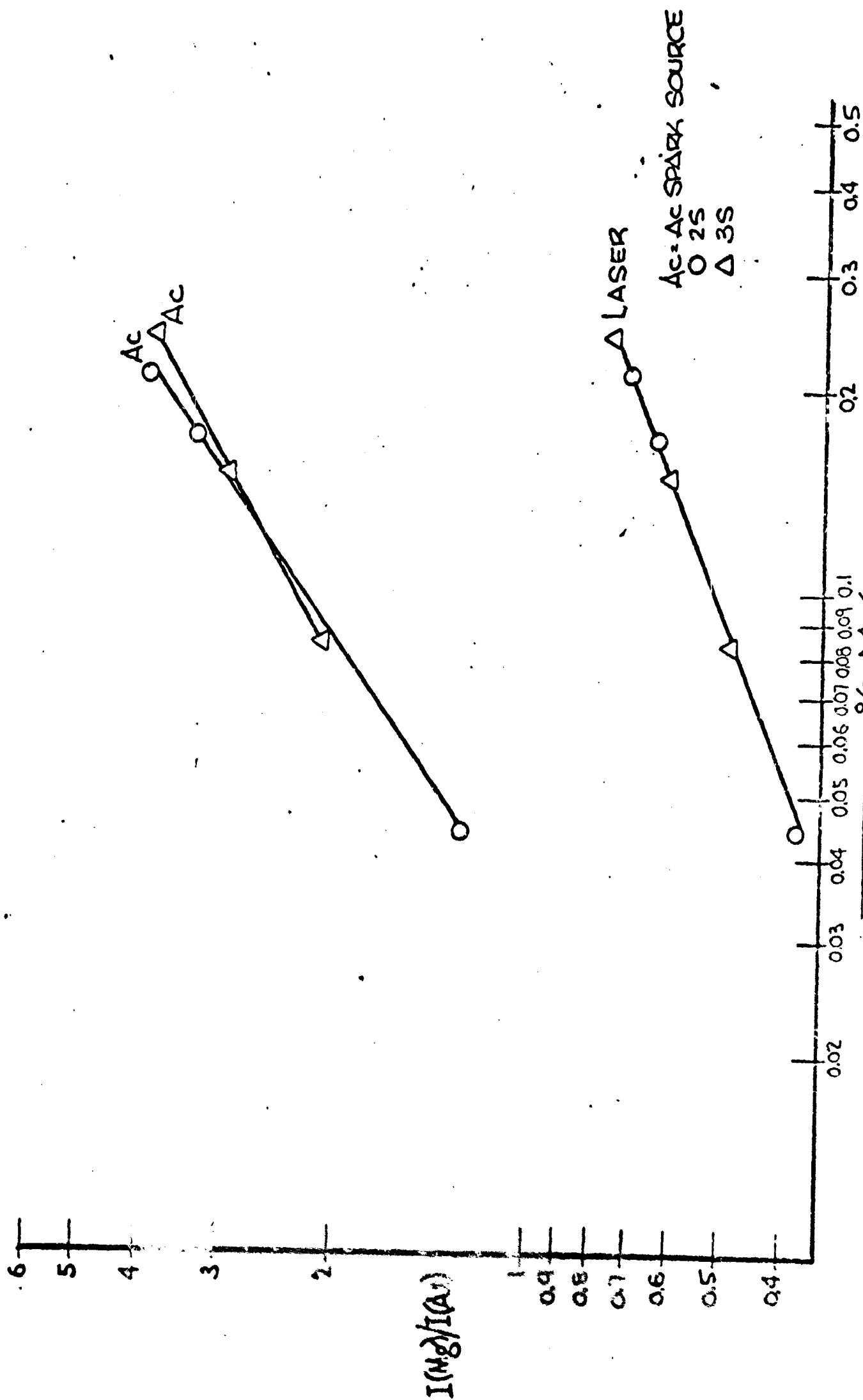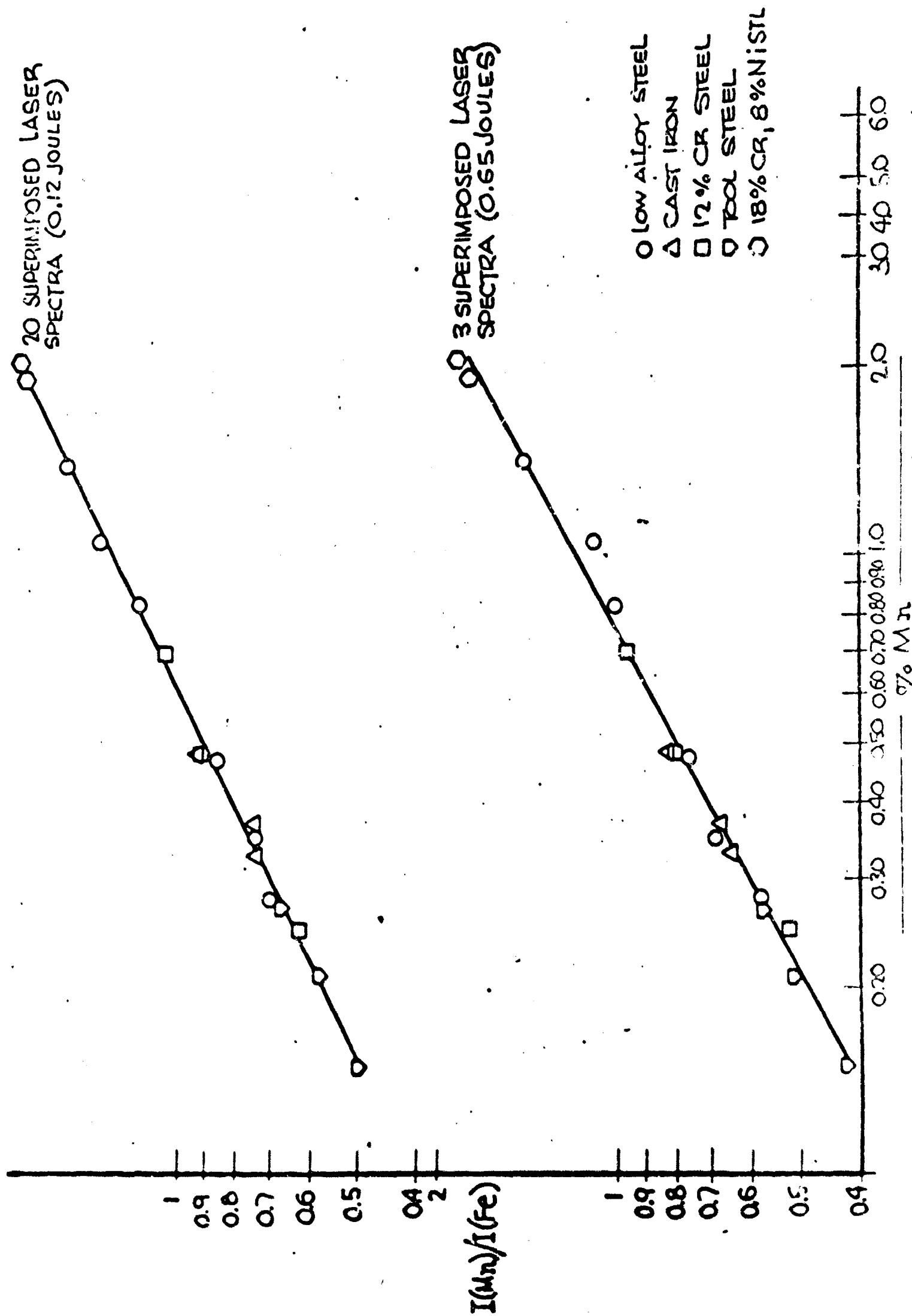
Figure 11C Quantitative analysis of Mg in aluminum alloys with an AC spark and a laser excitation source
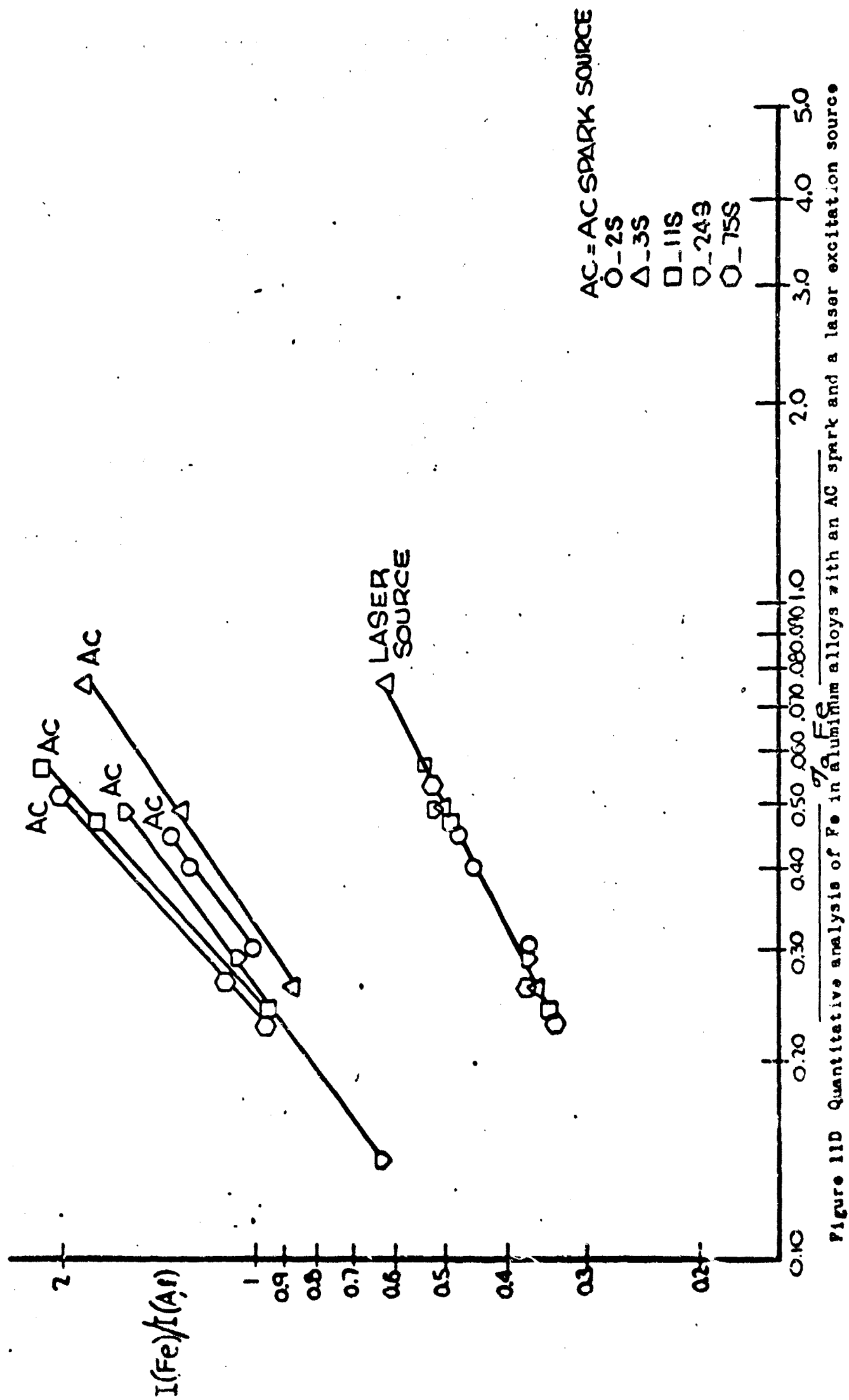
Figure 11D Quantitative analysis of Fe in aluminum alloys with an AC spark and a laser excitation source
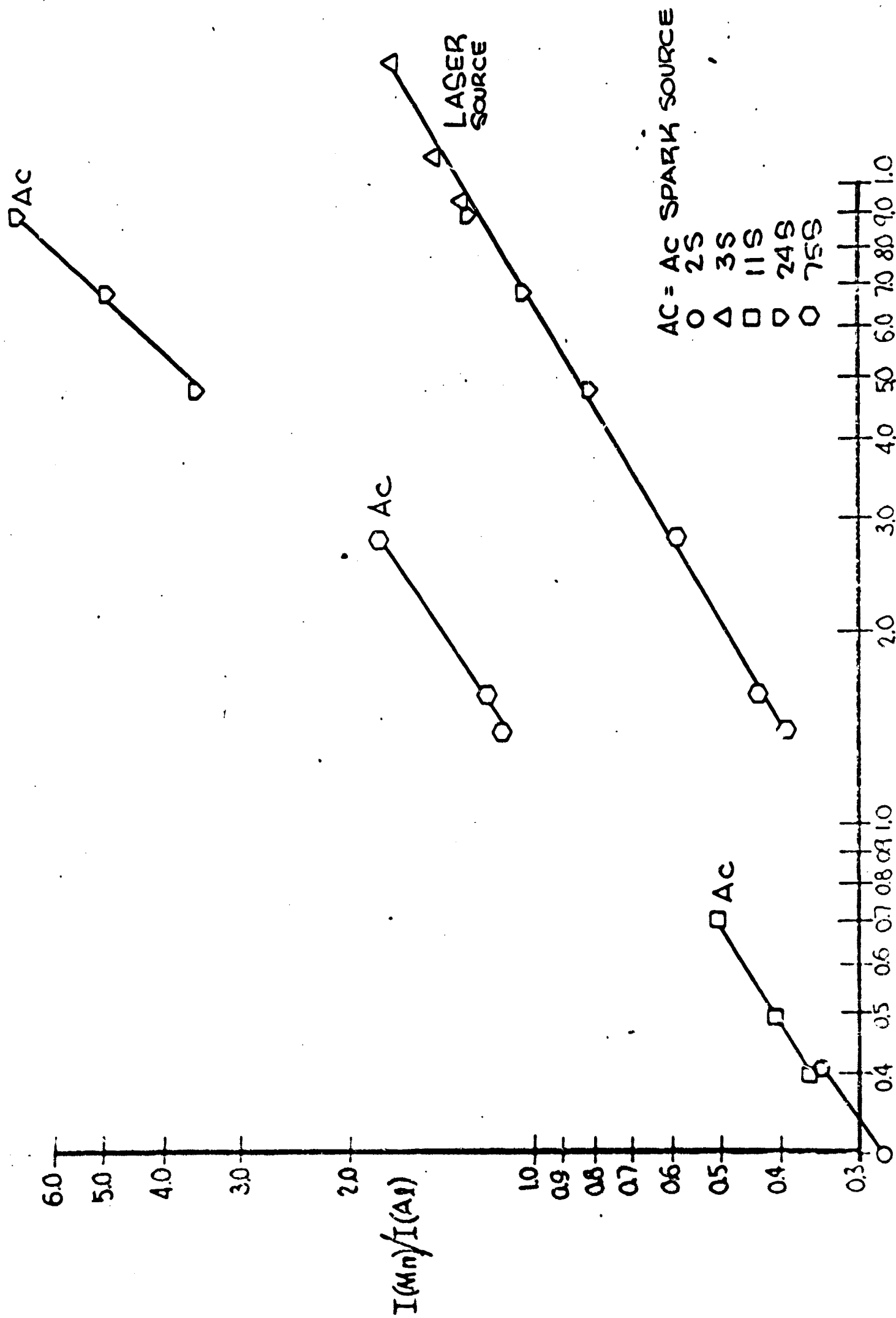
Figure 11E Quantitative analysis of Mn in aluminum alloys with an AC spark and a laser excitation source

Figure 12A Quantitative analysis of Mn in iron alloys with single (0.12 joules) and multiple pulse (0.65 joules) laser beam

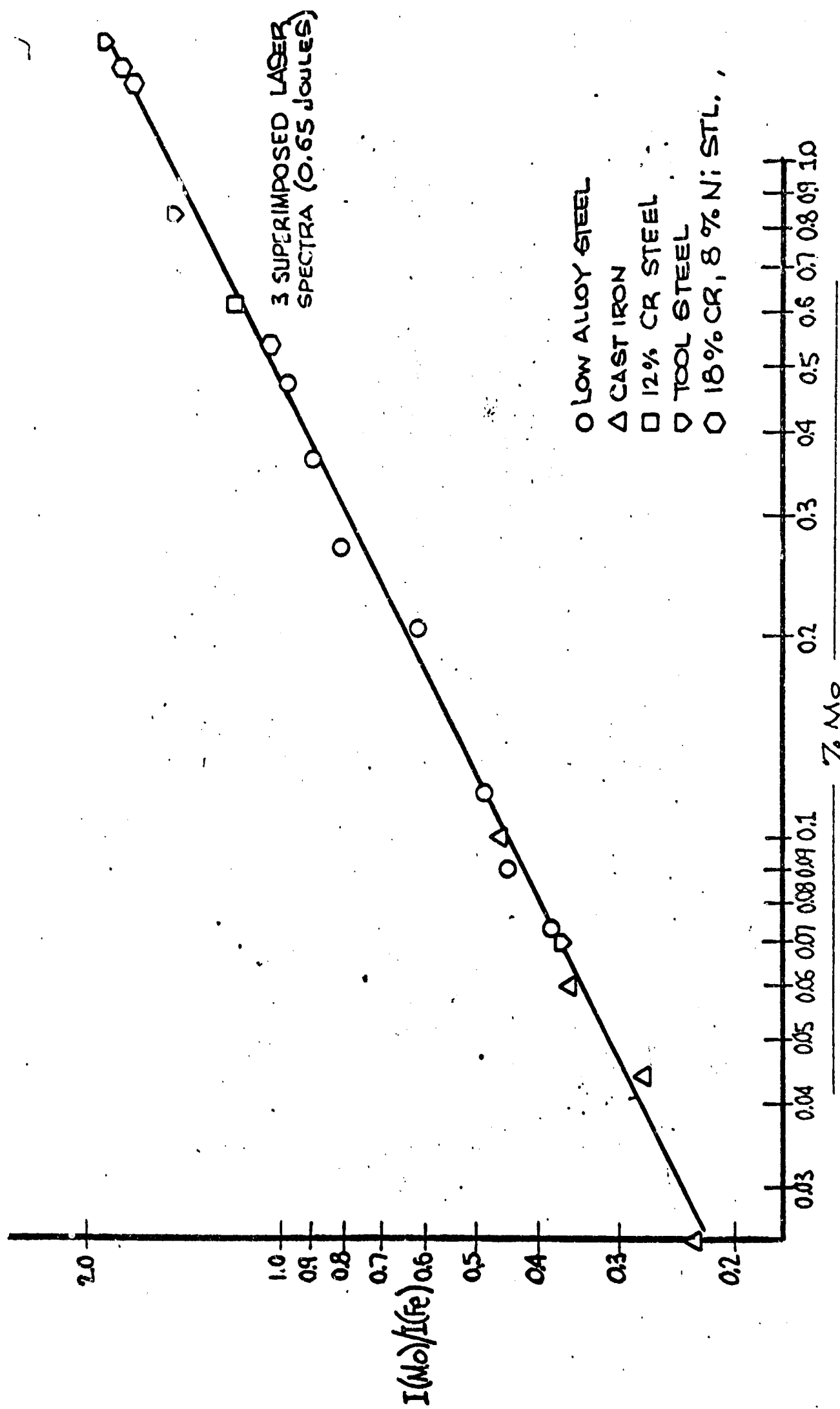20 SUPERIMPOSED LASER SPECTRA (0.12 JOULES)

3 SUPERIMPOSED LASER SPECTRA (0.65 JOULES)

○ LOW ALLOY STEEL
△ CAST IRON
□ 12% CR STEEL
◊ TOOL STEEL
⬡ 18% CR, 8% Ni STL

% Mn

$I(Mn)/I(Fe)$
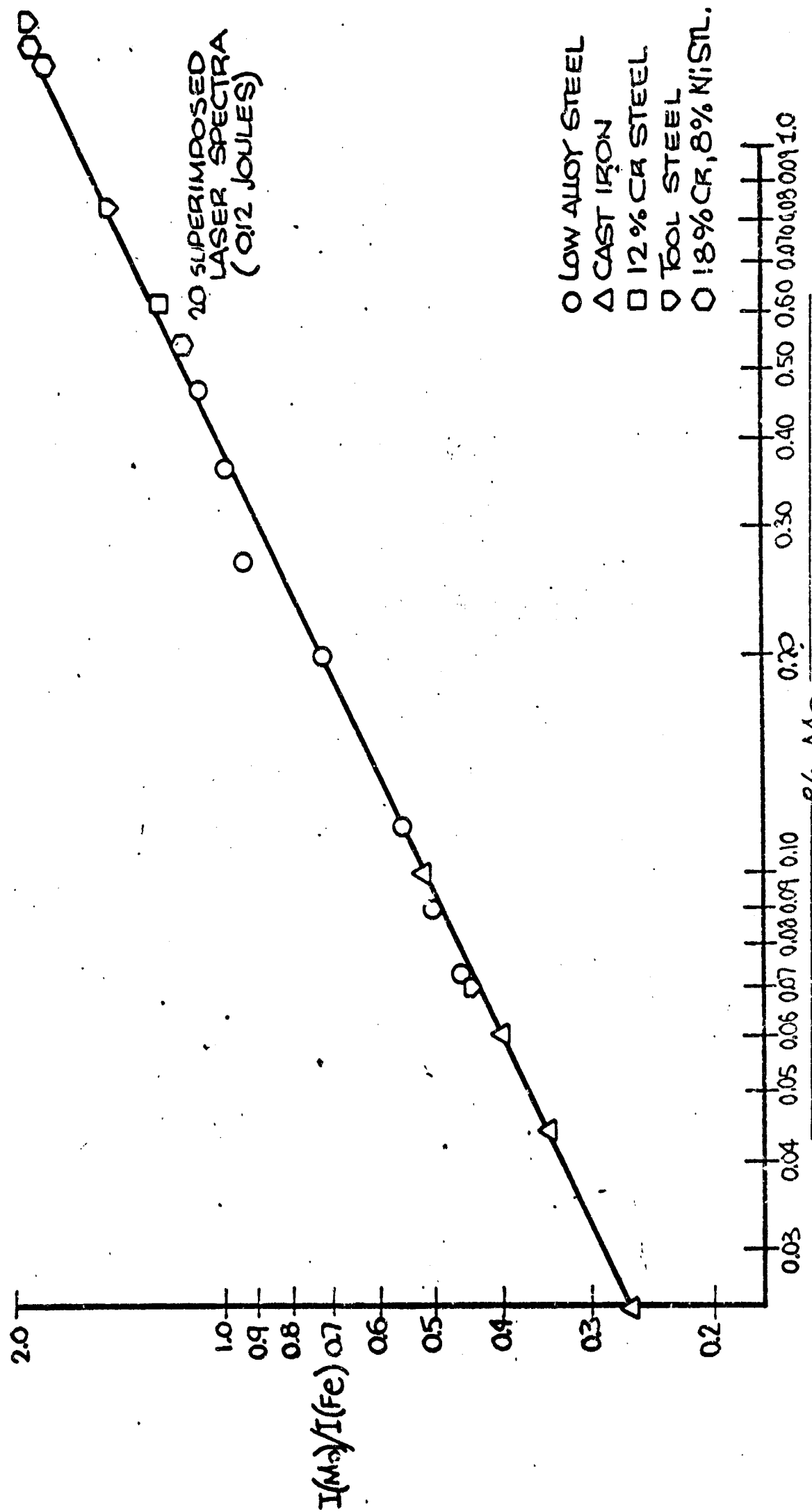
Figure 12B Quantitative analysis of Mo in iron alloys with single (0.12 joules) and multiple pulse
(0.65 joules) laser beams

3 SUPERIMPOSED LASER SPECTRA (0.65 JOULES)

○ LOW ALLOY STEEL
△ CAST IRON
□ 12% CR STEEL
▽ TOOL STEEL
⬡ 18% CR, 8% Ni STL.

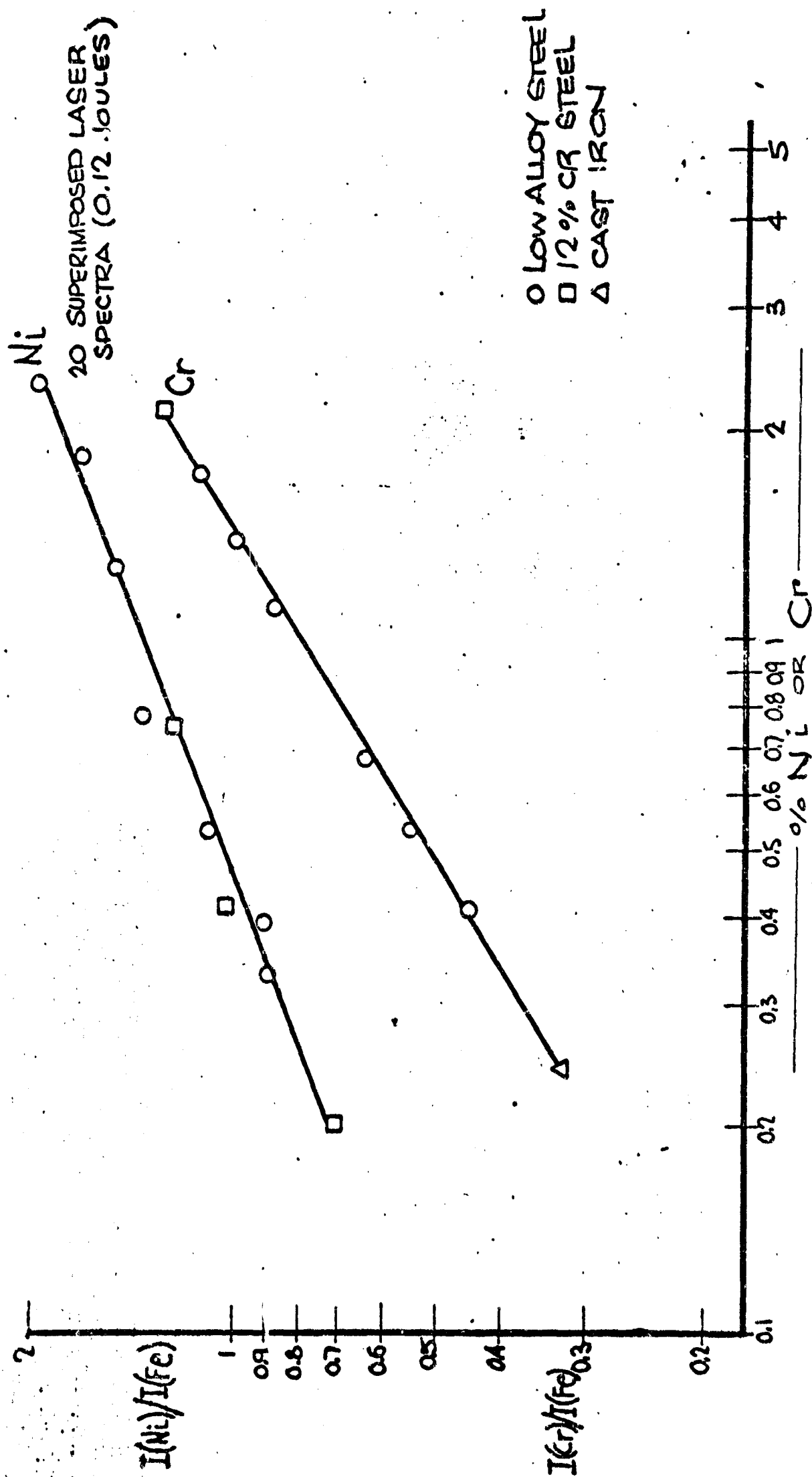$I(\text{Mo})/I(\text{Fe})$

% Mo

Figure 12B Continued

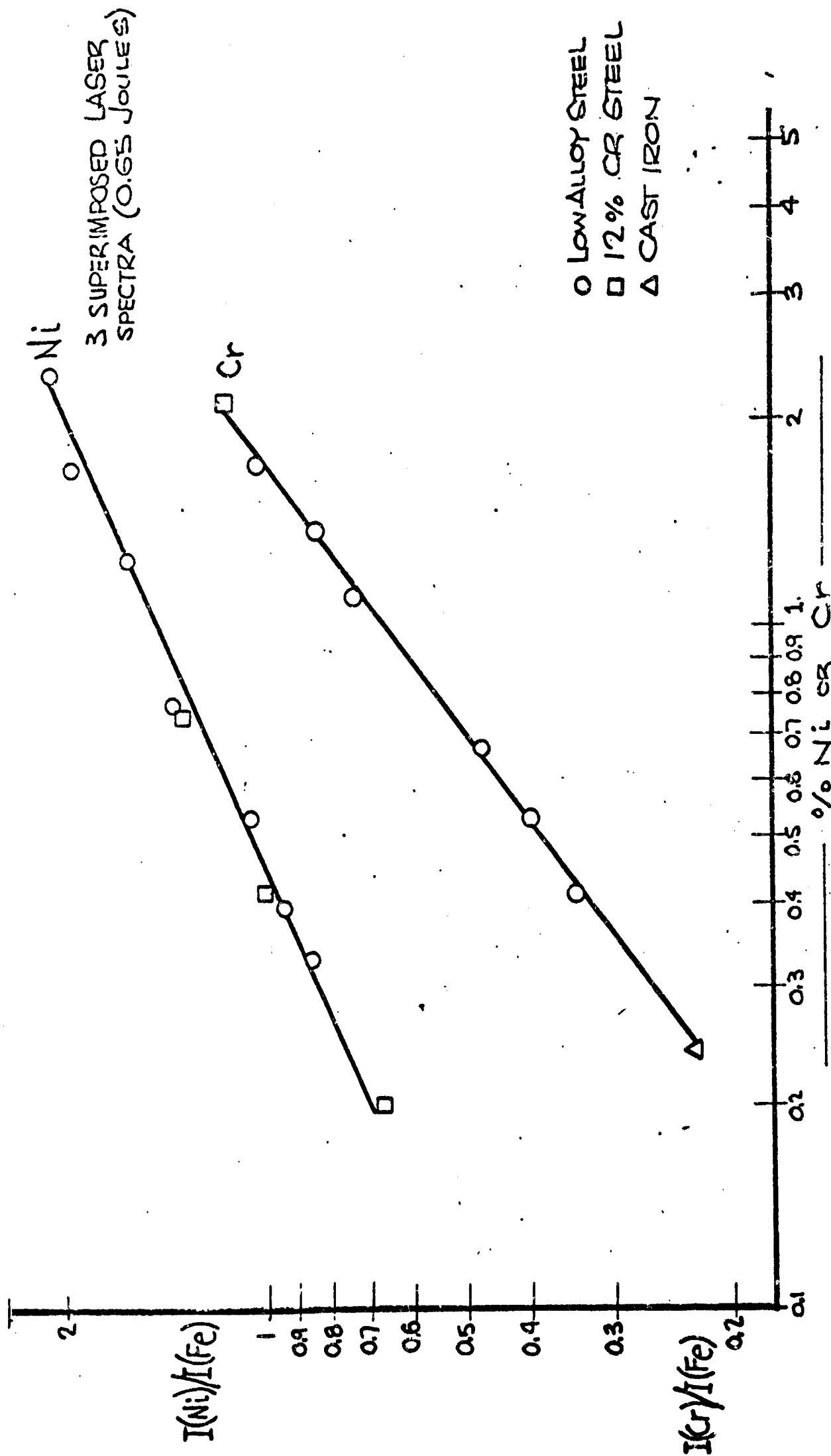Figure 12C   Quantitative analysis of Ni and Cr in iron alloys with a single pulse (0.12 joules) laser beam

Figure 12D Quantitative analysis of Ni and Cr in iron alloys with a multiple pulse (0.65 joules) laser beam
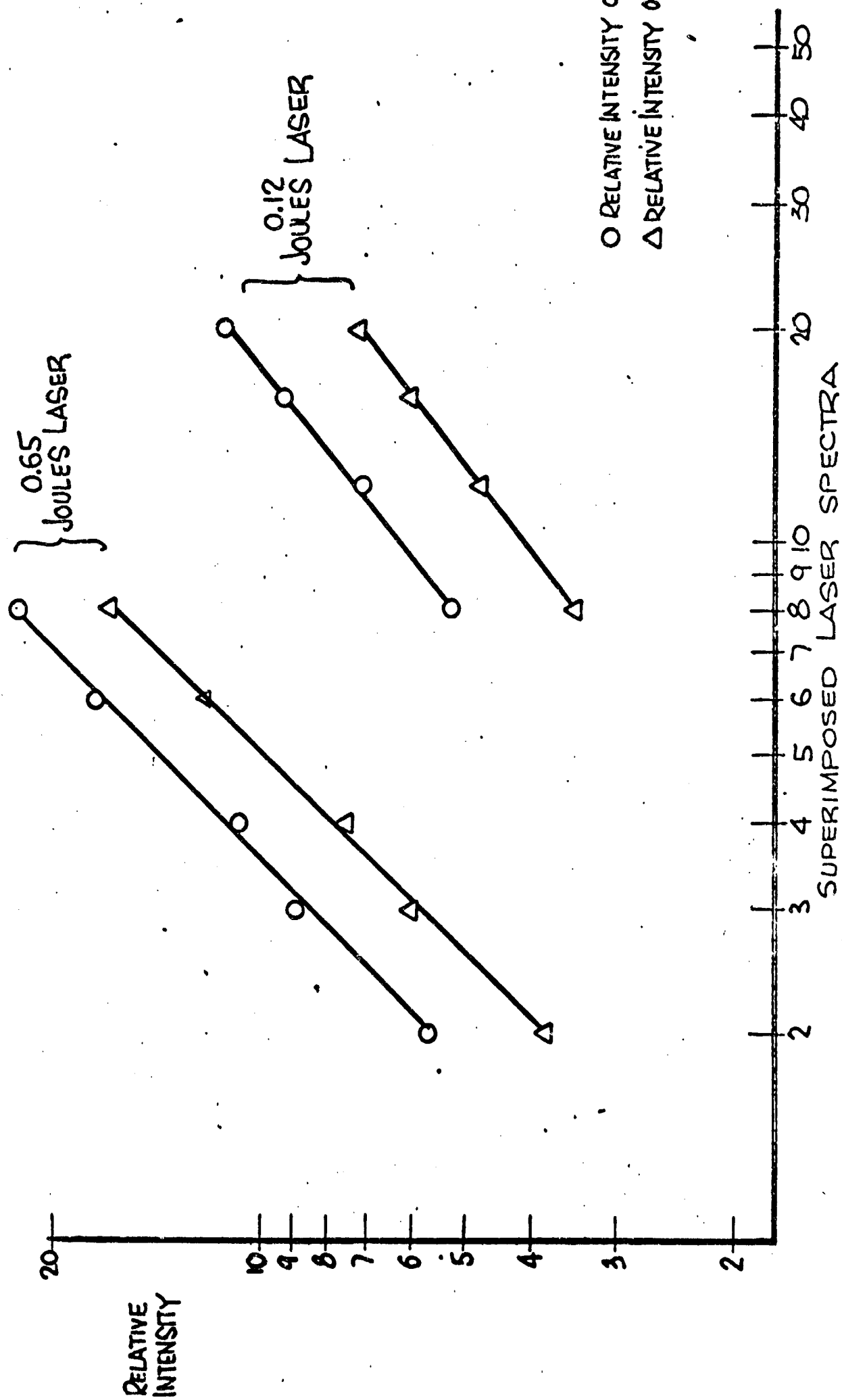
Figure 13 Relative intensity ratio as a function of superimposed laser spectra

REFERENCES CITED

1.   Brech, F., Devanney, J.J., Tabeling, R.W., Paper 19, Eastern Analytical Symposium, New York (Nov., 1962).

2.   Cotton, F., and Wilkinson, F., Advanced Inorganic Chemistry, John Wiley, New York, 1962.

3.   Maiman, T.H., Nature 187, 493, 1960.

4.   Hellworth, R. W., McClung, F.J., J. Appl. Phys. 33, 828, 1962.

5.   Honig, R.E., RCA Review 18 (June, 1957).

6.   Zaidel, A.N., Prokof Ev, V.K., Raiskii, S.M., Tables of Spectrum Lines, Pergamon Press, New York, 1961.

7.   Corliss, C.H., Bozman, W.R., Experimental Transition Probabilities for Spectral Lines of Seventy Elements, NBS MOnogram 53, U.S. Government Printing Office, Washington, D.C., 1962.

8.   Howe, J.A., J. Chem. Phys. 39, 1962, 1963.

9.   Honig, R.E., and Woolston, J.R., Appl. Phys. Letters 2, 138, 1962

10.   Honig, R.E., Appl. Phys. Letters 3,8, 1963.

11.   Ready, J.F., J. Appl. Phys. 36, 462, 1965.

12.   Ready, J.F., Appl. Phys. Letters 3, 11, 1963.

13.   Spex Speaker 8 (Oct., 1963).

14.   Crosswhite, H.M., Steinhaus, A.W., and Kieke, G.H., J. Opt. Soc. Am. 43, 257, 1953.

15.   Youden, W.J., Statistical Methods for Chemists, John Wiley, New York, 1959.

16.   Weast, R.C., Selby, S.M., and Hodgman, C.D., Handbook of Chemistry and Physics, Chemical Rubber Co., Cleveland, Ohio.

17.   Herzberg, G., Atomic Spectra and Atomic Structure, Dover, New York, 1944.

DOCUMENT CONTROL DATA - R&D

(Security classification of title, body of abstract and indexing annotation must be entered when the overall report is classified)

1. ORIGINATING ACTIVITY *(Corporate author)*	2a. REPORT SECURITY CLASSIFICATION
Boston College	Unclassified
Chestnut Hill, Massachusetts 02167	2b. GROUP

3. REPORT TITLE

An Investigation of Properties of The Laser Microprobe

4. DESCRIPTIVE NOTES *(Type of report and inclusive dates)*

Final report (Part I)   Scientific   1 July 1964–13 August 1965

5. AUTHOR(S) *(Last name, first name, initial)*

DEVLIN, James J., S.J. and LA CONTI, Anthony B.

Approved
20 Dec. 1905

6. REPORT DATE	7a. TOTAL NO. OF PAGES	7b. NO. OF REFS
13 August 1965	83	1

8a. CONTRACT OR GRANT NO.	9a. ORIGINATOR'S REPORT NUMBER(S)
AF19(604)-8819	
b. PROJECT AND TASK NO.	
5620-03	
c. DOD ELEMENT	9b. OTHER REPORT NO(S) *(Any other numbers that may be assigned this report)*
61445014	
d. DOD SUBELEMENT	AFCRL-65-855 (I)
681301	

10. AVAILABILITY/LIMITATION NOTICES Qualified requestors may obtain copies of this report from DDC. Other persons or organizations should apply to the Clearinghouse for Federal Scientific and Technical Information (CFSTI), Sills Building, 5285 Port Royal Road, Springfield, Virginia 22151

11. SUPPLEMENTARY NOTES	12. SPONSORING MILITARY ACTIVITY
	Hq. AFCRL, OAR (CRW)
	United States Air Force
	L. G. Hanscom Field, Bedford, Mass.

13. ABSTRACT The Laser Microprobe as a source for emission spectrochemical analysis has been investigated. A study is made of the mechanisms and factors entering into the interaction and excitation processes which affect quantitative analysis by the laser. The results of a quantitative analysis of aluminum and iron alloys performed with the ruby laser as an excitation source are discussed. The size and character of laser-produced craters in a number of pure/metals element was investigated and the information gained thereby is used to help construct a model for the interaction and excitation process. The model holds for both single and multiple pulse operations. A study is made of the factors which control the pulse shape and power of a laser beam. Measuring equipment is depicted which allows the laser pulse and power to be monitored without significantly affecting the laser light used for excitation. A quantitative analysis of aluminum and iron alloys is achieved with the laser excitation source. The working curve resulting from laser excitation of aluminum alloys are compared to those obtained from a conventional AC spark source. A quantitative analysis of iron alloys is performed with both a single and multiple pulse laser beam.

DD FORM 1 JAN 64 1473

14. KEY WORDS	LINK A		LINK B		LINK C	
	ROLE	WT	ROLE	WT	ROLE	WT
Laser Microprobe	8, 9	3				
Emission Spectroscopy	8	3				
Spectrochemical Analysis	8	3				
Laser Beam			10	2		
Excitation Source			10, 6	2		
Crater Size and Characters			8, 7	3		
Laser Pulse Shape			6	2		
Laser Power			6	2		
Iron & Aluminum Alloys					1	2
Single Pulse Laser					10, 7	2
Multiple Pulse Laser					10, 7	2
Quantitative Analysis					10, 8	3

INSTRUCTIONS

1. ORIGINATING ACTIVITY: Enter the name and address of the contractor, subcontractor, grantee, Department of Defense activity or other organization (corporate author) issuing the report.

2a. REPORT SECURITY CLASSIFICATION: Enter the over-all security classification of the report. Indicate whether "Restricted Data" is included. Marking is to be in accordance with appropriate security regulations.

2b. GROUP: Automatic downgrading is specified in DoD Directive 5200.10 and Armed Forces Industrial Manual. Enter the group number. Also, when applicable, show that optional markings have been used for Group 3 and Group 4 as authorized.

3. REPORT TITLE: Enter the complete report title in all capital letters. Titles in all cases should be unclassified. If a meaningful title cannot be selected without classification, show title classification in all capitals in parenthesis immediately following the title.

4. DESCRIPTIVE NOTES: If appropriate, enter the type of report, e.g., interim, progress, summary, annual, or final. Give the inclusive dates when a specific reporting period is covered.

5. AUTHOR(S): Enter the name(s) of author(s) as shown on or in the report. Enter last name, first name, middle initial. If military, show rank and branch of service. The name of the principal author is an absolute minimum requirement.

6. REPORT DATE: Enter the date of the report as day, month, year, or month, year. If more than one date appears on the report, use date of publication.

7a. TOTAL NUMBER OF PAGES: The total page count should follow normal pagination procedures, i.e., enter the number of pages containing information.

7b. NUMBER OF REFERENCES: Enter the total number of references cited in the report.

8a. CONTRACT OR GRANT NUMBER: If appropriate, enter the applicable number of the contract or grant under which the report was written.

8b, 8c, & 8d. PROJECT NUMBER: Enter the appropriate military department identification, such as project number, subproject number, system numbers, task number, etc.

9a. ORIGINATOR'S REPORT NUMBER(S): Enter the official report number by which the document will be identified and controlled by the originating activity. This number must be unique to this report.

9b. OTHER REPORT NUMBER(S): If the report has been assigned any other report numbers (either by the originator or by the sponsor), also enter this number(s).

10. AVAILABILITY/LIMITATION NOTICES: Enter any limitations on further dissemination of the report, other than those imposed by security classification, using standard statements such as:

(1) "Qualified requesters may obtain copies of this report from DDC."

(2) "Foreign announcement and dissemination of this report by DDC is not authorized."

(3) "U. S. Government agencies may obtain copies of this report directly from DDC. Other qualified DDC users shall request through

_____."

(4) "U. S. military agencies may obtain copies of this report directly from DDC. Other qualified users shall request through

_____."

(5) "All distribution of this report is controlled. Qualified DDC users shall request through

_____."

If the report has been furnished to the Office of Technical Services, Department of Commerce, for sale to the public, indicate this fact and enter the price, if known.

11. SUPPLEMENTARY NOTES: Use for additional explanatory notes.

12. SPONSORING MILITARY ACTIVITY: Enter the name of the departmental project office or laboratory sponsoring (paying for) the research and development. Include address.

13. ABSTRACT: Enter an abstract giving a brief and factual summary of the document indicative of the report, even though it may also appear elsewhere in the body of the technical report. If additional space is required, a continuation sheet shall be attached.

It is highly desirable that the abstract of classified reports be unclassified. Each paragraph of the abstract shall end with an indication of the military security classification of the information in the paragraph, represented as (TS), (S), (C), or (U).

There is no limitation on the length of the abstract. However, the suggested length is from 150 to 225 words.

14. KEY WORDS: Key words are technically meaningful terms or short phrases that characterize a report and may be used as index entries for cataloging the report. Key words must be selected so that no security classification is required. Identifiers, such as equipment model designation, trade name, military project code name, geographic location, may be used as key words but will be followed by an indication of technical context. The assignment of links, rules, and weights is optional.